JOURNAL OF GEOPHYSICAL RESEARCH, VOL. 113, B09411, doi:10.1029/2007JB005398, 2008

Dynamics of a velocity strengthening fault region: Implications for slow earthquakes and postseismic slip

Hugo Perfettini[1] and Jean-Paul Ampuero[2]

Received 24 September 2007; revised 7 May 2008; accepted 2 July 2008; published 26 September 2008.

[1] We consider the effect of permanent stress changes on a velocity strengthening rate-and-state fault, through numerical simulations and analytical results on 1-D, 2-D, and 3-D models. We show that slip transients can be triggered by perturbations of size roughly larger than $L_b = G\, d_c/b\sigma$, where G is the shear modulus, d_c and b are the characteristic slip distance and the coefficient of the evolution effect of rate-and-state friction, respectively, and σ is the effective normal stress. Perturbations that increase the Coulomb stress lead to the strongest transients, but creep bursts can also be triggered by perturbations that decrease the Coulomb stress. In the latter case, peak slip velocity is attained long after the perturbation, so that it may be difficult in practice to identify their origin. The evolution of slip in a creep transient shares many features with the nucleation process of a rate-and-state weakening fault: slip initially localizes over a region of size not smaller than L_b and then accelerates transiently and finally expands as a quasi-static propagating crack. The characteristic size L_b implies a constraint on the grid resolution of numerical models, even on strengthening faults, that is more stringent than classical criteria. In the transition zone between the velocity weakening and strengthening regions, the peak slip velocity may be arbitrarily large and may approach seismic slip velocities. Postseismic slip may represent the response of the creeping parts of the fault to a stress perturbation of large scale (comparable to the extent of the main shock rupture) and high amplitude, while slow earthquakes may represent the response of the creeping zones to a more localized stress perturbation. Our results indicate that superficial afterslip, observed at usually seismogenic depths, is governed by a rate-strengthening rheology and is not likely to correspond to stable weakening zones. The predictions of the full rate-and-state framework reduce to a pure velocity strengthening law on a timescale longer than the duration of the acceleration transient, only when the triggering perturbation extends over length scales much larger than L_b.

Citation: Perfettini, H., and J.-P. Ampuero (2008), Dynamics of a velocity strengthening fault region: Implications for slow earthquakes and postseismic slip, *J. Geophys. Res.*, *113*, B09411, doi:10.1029/2007JB005398.

1. Introduction

[2] Since the advent of continuous GPS and dense strainmeter networks, the role of the slow portions of active faults has been highlighted by high-resolution observations of postseismic slip, transient creep episodes, and silent (or slow) earthquakes. Postseismic slip is often observed after large earthquakes, in all type of tectonic settings (crustal and subduction earthquakes), and can be considered as a general feature of the seismic cycle. In some cases postseismic moment can even exceed the coseismic moment [*Yagi et al.*, 2003]. During the postseismic period, slip rate decays roughly in inverse proportion to time, with typical durations of a few years and slip mostly located immediately below the seismogenic zone of the fault. Postseismic slip seems to be principally controlled by the dynamics of the transition region that connects the brittle zone of the fault to the ductile zone at greater depth and higher temperature, roughly between the isotherms 250°C and 450°C [*Blanpied et al.*, 1995; *Perfettini and Avouac*, 2004]. Ample evidence is provided by the postseismic slip of the 1992 Landers earthquake [*Savage and Svarc*, 1997; *Fialko*, 2004], the 1999 Chi-Chi earthquake [*Hsu et al.*, 2002], the 1999 Izmit earthquake [*Burgmann et al.*, 2002], the 1995 Antofagasta earthquake [*Chlieh et al.*, 2004], and the 2004 Sumatra sequence [*Chlieh et al.*, 2007; *Hsu et al.*, 2006]. Shallower afterslip is sometimes significant and has been observed in areas and depth ranges that are commonly thought as seismogenic [*Miyazaki et al.*, 2004; *Chlieh et al.*, 2007, 2008; *Hsu et al.*, 2006; *Pritchard and Simons*, 2006b].

[3] Slow slip transients, lasting from days to years (A. Lowry et al., The fault slip budget in Guerrero, southern

[1]Institut de Recherche pour le Développement, Laboratoire des Mécanismes de Transfert en Géologie, Toulouse, France.
[2]Seismological Laboratory, California Institute of Technology, Pasadena, California, USA.

0148-0227/08/2007JB005398$09.00

Mexico, unpublished manuscript, 2008), involving slip rates as large as 100 cm a^{-1} [*Miyazaki et al.*, 2006], have now been observed in the Cascadia subduction zone [*Dragert et al.*, 2001], in northern California [*Miller et al.*, 2002; *Szeliga et al.*, 2004], in Mexico [*Lowry et al.*, 2001], on the San Andreas fault [*Linde et al.*, 1996], in Japan [*Hirose et al.*, 1999; *Ozawa et al.*, 1997; *Katsumata et al.*, 2002; *Miyazaki et al.*, 2006], in New Zealand [*Douglas et al.*, 2005], and in Italy [*Crescentini et al.*, 1999]. As for postseismic slip, slow earthquakes are observed not only in subduction zones but on all type of active faults, and their slip is located at the brittle/ductile transition zone of the fault. One of the most intriguing features of some of these slow earthquakes is their very regular periodicity, in particular in Cascadia [*Rogers and Dragert*, 2003]. Moreover, their occurrence often coincides with nonvolcanic seismic tremor [*Obara*, 2002; *Rogers and Dragert*, 2003; *Obara et al.*, 2004], probably induced by fluid circulation [*Chouet*, 1992; *Kao et al.*, 2005]. It has been suggested that tremors in subduction faults have a metamorphic origin [*Rogers and Dragert*, 2003; *Szeliga et al.*, 2004] because of the abundance of fluids associated to the dehydration process of the slab, but this is less clear for the similar tremors observed on the San Andreas fault [*Nadeau and Dolenc*, 2005]. Deep low-frequency earthquakes have also been observed in coincidence with tremor and episodic slow slip in subduction zones, with focal mechanism and location consistent with interplate slip [*Shelly et al.*, 2006, 2007]. An emerging view [*Dragert*, 2007; *Ito et al.*, 2007] is that the slow slip transient, which propagates on a creeping section of the fault, breaks isolated brittle asperities on its way producing localized low-frequency earthquakes and squeezes fluids out producing diffused tremor activity on and above the plate interface. In this view the slow slip transient, whatever its origin, takes a prominent role.

[4] This article explores mechanical models of slip transients based on laboratory-derived friction laws. One-dimensional models of the relaxation of a fault region with velocity strengthening frictional properties, in response to the sudden stress change induced by the main shock, provide a fair description of postseismic deformation time series [*Marone et al.*, 1991; *Perfettini and Avouac*, 2004; *Perfettini et al.*, 2005]. Three-dimensional numerical models have been successful in modeling the postseismic GPS deformation field of the Izmit [*Hearn et al.*, 2002] and Landers earthquakes [*Perfettini and Avouac*, 2007]. These models assume a rate-strengthening rheology where stress changes $\Delta\tau$ are related to deformation rate $\dot{\epsilon}$ through

$$\Delta\tau = A \ln \dot{\epsilon} \tag{1}$$

where $A > 0$. Such a relation is verified by an interface sliding in steady state under rate-and-state friction [*Dieterich*, 1979; *Ruina*, 1983] with $A = \sigma(a - b)$, where b and a are two frictional parameters, and σ is the effective normal stress. Equation (1) is also characteristic of a large class of thermally activated processes such as diffusion creep, dislocation creep [*Turcotte and Schubert*, 2002], or pressure solution creep [*Shimizu*, 1995], which could be active in the temperature range of the transition zone. The rate and state formalism may also be interpreted as a thermally activated process [*Nakatani*, 2001]. Therefore, even if the real deformation law was a mixture of rate-and-state friction and for example pressure-solution creep, the overall law will still keep the form of equation (1), where A is a lumped parameter associated with all those competing processes.

[5] As in previous modeling approaches [*Liu and Rice*, 2005], we will consider faults governed by the laboratory motivated rate-and-state friction laws [*Dieterich*, 1979; *Ruina*, 1983; *Marone*, 1998], for which the brittle/ductile rheological transition corresponds to the transition from velocity-weakening to velocity-strengthening behavior. We discuss in section 5.5 possible extensions of our results to other type of rheologies such as power law creep. Rather than studying specific geometries and friction parameter distributions we focus on simple canonical cases, for which the vast parameter space can be explored exhaustively, and for which analytical or asymptotic solutions can be obtained in closed form to provide a physical insight into different possible scenarios.

[6] The remainder of this article is organized as follows. In section 2 we introduce the basic assumptions of our models. In section 3 we summarize previous results on earthquake nucleation on rate-and-state weakening faults. In section 4 these results are extended to strengthening faults, and we study systematically their response to abrupt stress perturbations. In particular we show that in contrast to the classical expectation that strengthening faults are stable, strong slip acceleration transients can be generated there, even by apparently unfavorable (negative) loads. Section 4.3 summarizes important analytical results. Section 5 discusses their implications on the properties of postseismic slip and slow earthquakes.

2. Model Formulation

[7] We consider a fault governed by rate-and-state friction embedded in a linear elastic crust. We do not attempt to include in the model all the geometrical features associated with subduction faults. We rather focus on a basic canonical geometry, a planar fault embedded in an unbounded elastic medium. In particular we exclude the free surface and the normal stress changes it might induce on the fault because it is a second-order effect at the depth range we are interested in. We also neglect rake rotations and, in our 3-D models, we consider only the along-dip components of stress and slip. The crust is assumed homogeneous and isotropic, with shear modulus G and shear wave speed c_s.

[8] We adopt the usual quasi-dynamic approximation [*Rice*, 1993]. The shear stress $\tau(\mathbf{r}, t)$ at a point $\mathbf{r}$ on the fault and time t is related to the stress $\tau_0(\mathbf{r}, t)$ resulting from external loads, to the current slip rate $V(\mathbf{r}, t)$ and to the spatial distribution of slip $D(\mathbf{r}, t)$ by

$$\tau(\mathbf{r}, t) = \tau_0(\mathbf{r}, t) - \frac{G}{2c_s} V(\mathbf{r}, t) - K[D](\mathbf{r}, t), \tag{2}$$

The second term of the right-hand side is the so-called radiation damping term describing the instantaneous elastodynamic response to changes of V. The last term encapsulates the elastostatic stress transfer along the fault induced by spatially nonuniform slip. It is a linear

Table 1. Reference Model Parameters

Variable	Value
μ_*	0.6
V_{pl}	10^{-9} m
G	30 GPa
ν	0.25
c_s	3 km/s
σ	100 MPa
b	0.01

integral operator, derived from a representation theorem, e.g., in 3-D:

$$K[D](\mathbf{r},t) = \int\int_{\Gamma} K(\mathbf{r},\mathbf{r}')D(\mathbf{r}',t)\, d^2\mathbf{r}' \tag{3}$$

where the integral is taken over the fault surface Γ and the kernel $K(\mathbf{r}, \mathbf{r}')$ is the static fault shear stress a point r induced by slip at point $\mathbf{r}'$. We will selectively study 1-D, 2-D, and 3-D models, all of these embraced by equation (2) with a stiffness kernel K specific to each dimension. In the remainder we will drop the argument $(\mathbf{r}, t)$ when the context is unambiguous.

[9] In the rate-and-state formalism [*Ruina*, 1983] the shear stress is equated to the frictional strength:

$$\tau = \mu\sigma. \tag{4}$$

where σ is the effective normal stress on the fault and the friction coefficient μ is given by:

$$\mu = \mu_* + a\ln\left(\frac{V}{V_*}\right) + b\ln\left(\frac{\theta V_*}{d_c}\right). \tag{5}$$

where V is slip velocity; θ is a fault state variable; a, b, and d_c are constitutive parameters; and μ_* is the steady state friction coefficient at an arbitrarily fixed reference velocity V_*. Without loss of generality we choose $V_* = V_{pl}$ where V_{pl} is the long-term slip velocity. Because in the geometries we consider the normal stress is invariant the actual value of μ_* is irrelevant.

[10] Two empirical evolution laws for the state variable θ are in common use, the aging law [*Dieterich*, 1981]

$$\frac{d\theta}{dt} = 1 - \frac{V\theta}{d_c}, \tag{6}$$

and the slip law [*Ruina*, 1983]

$$\frac{d\theta}{dt} = -\frac{V\theta}{d_c}\ln\left(\frac{V\theta}{d_c}\right). \tag{7}$$

We will mostly present results obtained considering the aging law because it is much easier to deal with this law analytically and numerically, but the differences with the slip law will be discussed when relevant results are available. We emphasize that these laws are of empirical origin, based on laboratory observations. None of the two fits the ensemble of observations, although recent experimental results with large velocity jumps [*Bayart et al.*, 2006], as relevant at the tips of propagating ruptures, are in favor of the slip law. The most appropriate state evolution law for crustal faults is still uncertain.

[11] Steady-state sliding, $\dot{\theta} = 0$ and $\dot{V} = 0$, implies for both evolution laws $\theta = d_c/V$ and

$$\mu = \mu_* + (a-b)\ln\left(\frac{V}{V_*}\right), \tag{8}$$

We define a dimensionless variable (a shorthand notation),

$$\Omega \doteq \frac{V\theta}{d_c}, \tag{9}$$

that quantifies how far or close from steady state a fault is $\Omega = 1$ corresponds to steady state sliding, $\Omega < 1$ and $\Omega > 1$ to sliding below and above steady state, respectively. The quantity Ω can be referred to as the "distance to steady state."

[12] Unless stated otherwise, the frictional properties are taken uniform along the fault. Although we will work with dimensionless quantities, typical values are given for reference in Table 1.

[13] The governing equations are solved numerically with the same approach as *Perfettini and Avouac* [2007] and *Rubin and Ampuero* [2005], among others. Equations (2) to (6) or (7) are spatially discretized on a regular Cartesian grid. The discrete version of the kernel K is computed using the analytical solutions of *Okada* [1992] in 3-D and using the spectral approach of *Cochard and Rice* [1997] in 2-D. The resulting system of ordinary differential equations are integrated in time by a fifth-order Runge-Kutta algorithm or the Bulirsch-Stoer algorithm, with adaptive time step [*Press et al.*, 1992].

[14] The grid spacing Δx is chosen as a small fraction of the length scale L_b (equation (10)) defined by *Rubin and Ampuero* [2005]. We typically set $\Delta x = L_b/20$ for the aging law and $\Delta x = L_b/200$ for the slip law. Whereas the criterion $\Delta x \ll L_b$ has been previously applied for rate-and-state weakening faults [*Hillers et al.*, 2007; *Ampuero and Rubin*, 2008], we show in Appendix A that it also applies to strengthening fault regions. We emphasize that, for usual values of a/b, this criterion for numerical resolution is more stringent than the one introduced by *Rice* [1993], which is based on the critical length scale L_c (equation (19)) and has been widely used in previous numerical work [e.g., *Liu and Rice*, 2005]. This is a critical issue close to stability transition zones, where $a/b \approx 1$, as illustrated in Figures A1 and A2.

3. Summary of Nucleation on Rate-and-State Faults

[15] Earthquake nucleation on faults governed by rate-and-state friction with velocity-weakening has been thoroughly studied by *Dieterich* [1992], *Rubin and Ampuero* [2005], and *Ampuero and Rubin* [2008]. On an infinitely long planar fault embedded in a 2-D elastic medium a perturbation from uniform sliding eventually leads to a seismic instability. Under the aging law, slip evolves through the following consecutive stages:

[16] 1. The first stage is early expansion. If the initial perturbation is broad and smooth, the nucleation zone

extends laterally, roughly until its size L satisfies $L/L_b \approx V_{out}/(V - V_{out})$, where $V_{out}(t)$ and $V(t)$ are slip rates outside and at the center of the perturbation, respectively, and

$$L_b \doteq \frac{Gd_c}{b\sigma} \tag{10}$$

This stage is not clearly observed under more heterogeneous initial conditions and involves weak slip rates that would be hard to detect geodetically.

[17] 2. The second stage is localization. The nucleation zone shrinks until it reaches a minimal size, not smaller than

$$L_\nu = 1.3774 L_b \tag{11}$$

The closer the minimal length gets to L_ν the farther above steady state the fault has been able to evolve. This in turn depends on the strength of the initial conditions and on a/b (the return to steady state is faster for higher a/b; see equation (16)).

[18] 3. The third stage is localized self-acceleration. Slip accelerates on a patch of fixed size L_ν. The evolution is identical to the self-acceleration of a spring block system far above steady state [*Dieterich*, 1994], with stiffness

$$K_\nu = 0.6219\, K_b \tag{12}$$

where

$$K_b \doteq G/L_b = b\sigma/d_c \tag{13}$$

For instance, if the tectonic loading rate is neglected an inverse time-to-failure singularity is obtained:

$$V(t) = \frac{V(0)}{1 - t/t^*}, \tag{14}$$

where $V(0)$ is the initial sliding velocity, the failure time being

$$t^* = 2.6448 \frac{a}{b} \frac{d_c}{V(0)} \tag{15}$$

Localized self-acceleration is possible for any value of a/b (even if $a > b$, as will be discussed later). However, the occurrence of a finite-time instability requires the fault to remain far above steady state. As shown by *Rubin and Ampuero* [2005], this can be accomplished only if $a/b > 0.3781$ because

$$\Omega \propto V^{1-2.6448\, a/b} \tag{16}$$

With reference to the spring block model the numerical factor in equations (15) and (16) can be expressed as $2.6448 = 1/(1 - K_\nu/K_b)$.

[19] 4. The fourth stage is quasi-static crack growth. If $a/b > 0.3781$, the nucleation zone eventually comes back close to steady state at its center and starts expanding, taking the form of a crack that grows up to a limit size

$$L_\infty = \frac{2}{\pi} \left(\frac{b}{b-a} \right)^2 L_b \tag{17}$$

The rupture speed V_{prop} is related to the peak slip rate at the crack tip $V_{\max}$ by *Ampuero and Rubin* [2008]:

$$V_{prop} \approx \frac{G}{b\sigma} \frac{V_{\max}}{\ln(V_{\max}\theta_i/d_c)} \tag{18}$$

where θ_i is the value of the state variable before the arrival of the rupture front.

[20] A fault segment is unstable if its size L is larger than a critical size that scales with

$$L_c \doteq \frac{Gd_c}{(b-a)\sigma} \tag{19}$$

This critical length scale is obtained from linear stability analysis in a infinitely long fault [*Ruina*, 1983; *Rice and Ruina*, 1983] and from nonlinear analysis of quasi-static spring block models [*Gu et al.*, 1984; *Ranjith and Rice*, 1999].

[21] Some aspects of nucleation depend on the chosen evolution law for the state variable or, more fundamentally, on how fracture energy scales with V. Under the slip law the main differences are [*Ampuero and Rubin*, 2008]:

[22] 1. During localization the nucleation patch keeps shrinking and its size L_b' is given by

$$L_b' = L_b (\ln V_{\max}\theta_i/d_c)^{-1}. \tag{20}$$

The contraction factor is at most of the order of 20, considering $V_{\max} \approx 1$ m/s and $\theta_i/d_c \approx V_{pl} = 45$ mm a^{-1}.

[23] 2. In the final stage the nucleation zone can take the form of a crack or a pulse, depending on details of initial conditions and background stress.

[24] 3. The transition from localized acceleration to quasi-static crack/pulse propagation occurs at higher a/b.

[25] 4. There is no limiting size L_∞.

4. Dynamics of a Rate-and-State Strengthening Fault

4.1. Response to Positive Coulomb Stress Perturbations

[26] We consider a rate-and-state strengthening region of a fault, a square patch of size $L = 15\ L_b$ with uniform friction properties ($b/a = 0.9$), surrounded by steady slip at prescribed velocity V_{pl}. Initially, the patch is sliding at steady state with slip rate V_{pl}. At $t = 0$ it is perturbed by an instantaneous step in shear stress with Gaussian spatial distribution:

$$\Delta\tau(x,z) = \Delta\tau_0 \exp\left(-\frac{x^2 + z^2}{2R_0^2} \right), \tag{21}$$

where x and z are the along-strike and along-dip positions, respectively, relative to the patch center.

[27] Figure 1 shows the evolution of the maximum sliding velocity $V_{\max}$ as a function of time, under the aging law (equation (6)), for $\Delta\tau_0 = 10\ a\sigma$ and $R_0 = 4\ L_b$. Slip velocity initially jumps, then accelerates, and finally relaxes back to V_{pl}. The transient acceleration phase is in contrast to the response of a pure velocity strengthening fault ($b = 0$) to

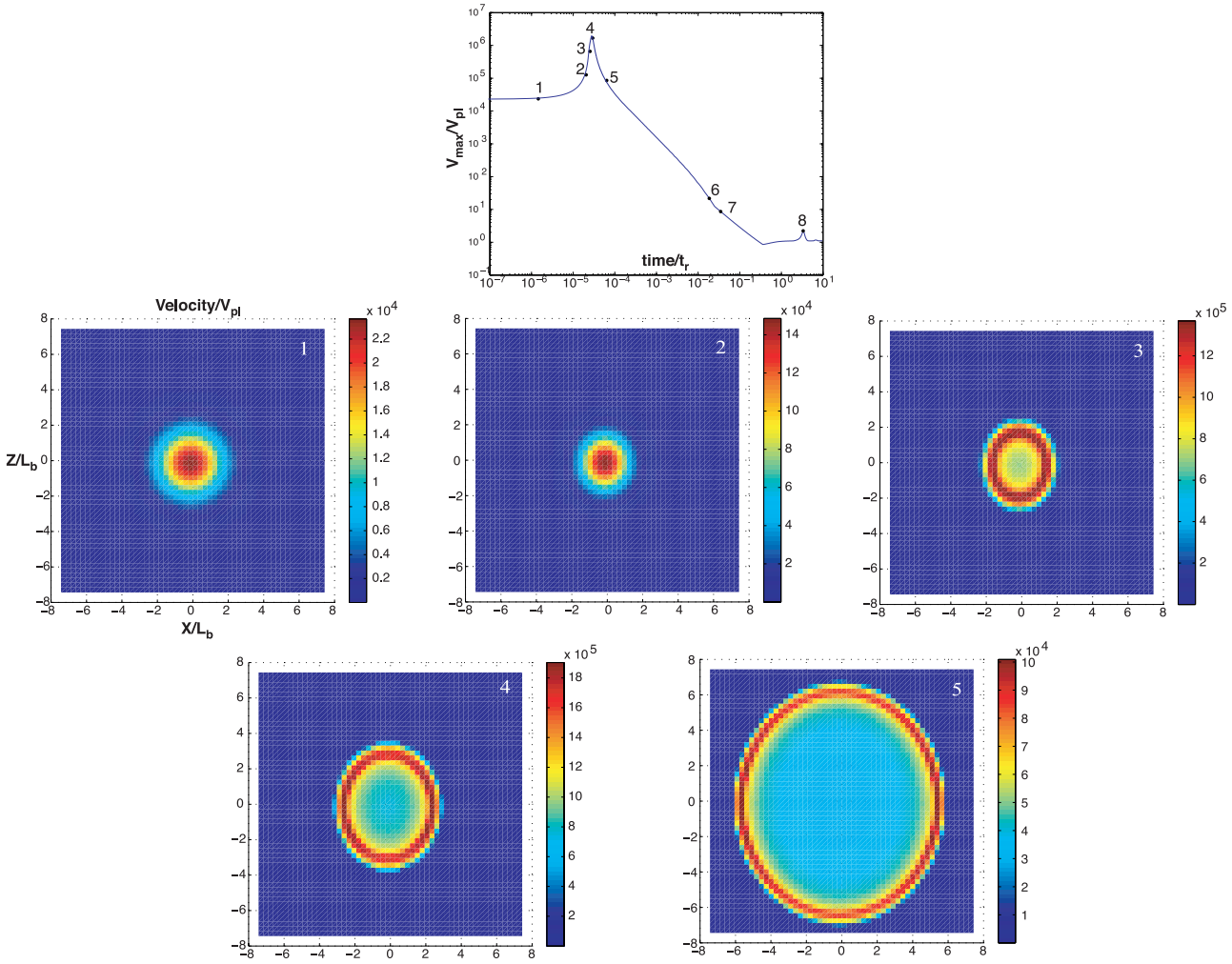

Figure 1. Evolution of slip velocity on a square fault patch following a stress perturbation of Gaussian shape, with characteristic length $R_0 = 4L_b$ and amplitude $\Delta\tau_0 = 10a\sigma$. (top) Evolution of the maximum slip velocity, with transient acceleration and subsequent relaxation. (bottom) Velocity snapshots (normalized by the loading velocity V_{pl}) at times indicated by labels in Figure 1 (top).

a stress step, for which $V_{\max}$ decreases monotonically [*Perfettini and Avouac*, 2007].

[28] Figure 1 also shows the spatial distribution of slip velocity at various times indicated by numbered labels in the $V_{\max}(t)$ plot. Slip acceleration is initially peaked at the patch center and concentrates on an area that shrinks down to a size of order L_b (snapshots 1 and 2). Close to the time of maximum velocity (snapshots 3 and 4) and during most of the relaxation stage (snapshot 5) slip spreads over the fault patch and velocity is peaked at the spreading front. After reaching the edges of the patch, the fronts are reflected back (points 6 and 7). Upon coalescence, they induce a secondary transient (point 8) of modest amplitude that vanishes for large L.

[29] The response of a strengthening fault to stress perturbations follows the same stages as the nucleation process of weakening faults summarized in section 3: slip localization, localized acceleration, and quasi-static crack propagation. In fact, as noted by *Rubin and Ampuero* [2005], the conditions leading to slip localization and acceleration are independent of the sign of $a - b$. A sufficient requirement is that the initial stress perturbation pushes the fault far enough above steady state ($\Omega \gg 1$). The main difference is that the strengthening fault eventually relaxes back to steady state, as expected from its intrinsic stability properties. The frustrated instability takes the appearance of a transient propagating creep episode.

[30] Figure 2 shows slip localization, acceleration (Figure 2, left) and crack propagation (Figure 2, right) on a 2-D simulation with similar parameters and initial conditions as in the previous 3-D example. Figure 3a shows the evolution of the propagation speed of the crack front, V_{prop}. The crack accelerates when it leaves the nucleation patch, driven mainly by the increasing stress drop induced by the relaxation to steady state inside the crack (on a strengthening fault stress decreases when slip decelerates). When the crack front moves beyond the edge of the region of initial stress excess it enters a region of negative stress drop and slows down. As shown in Figure 3a, during most of the transient V_{prop} and $V_{\max}$ are consistent with equation (39) where $\theta_i(x)$ is taken as the fault state at the onset of crack propagation (Figure 3b). Owing to the weak logarithmic dependence of

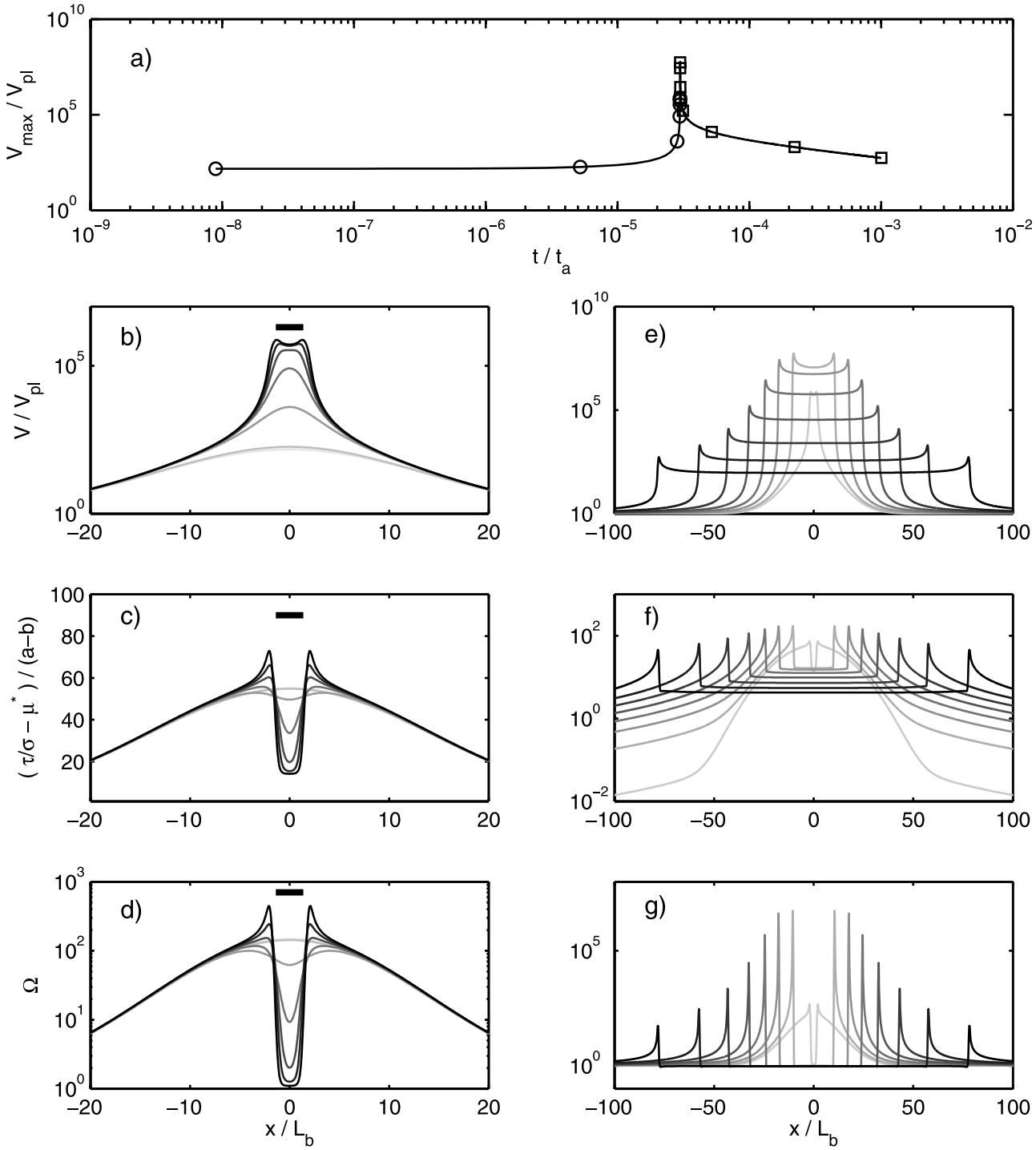

Figure 2. Evolution of a strengthening fault (a/b = 1.1) initially perturbed from uniform steady slip by a static stress step with Gaussian spatial distribution of length scale $20L_b$ and amplitude $5a\sigma$. Lighter curves are snapshots at earlier times. (a) Peak slip rate as a function of time. Slip rate, friction coefficient, and $\Omega = V\theta/d_c$ as a function of position along the fault during (b–d) slip localization, acceleration, and onset of crack growth and (e–g) during crack propagation. Snapshots times are respectively marked by circles and squares in Figure 2a. The thick bar in Figure s 2b–2d shows the theoretical nucleation size.

V_{prop} upon θ_i in equation (39), taking $\theta_i = d_c/V_{pl}$ yields also an appropriate estimate of V_{prop} outside the nucleation area:

$$V_{prop} \approx \frac{G}{b\sigma} \frac{V_{\max}}{\ln\left(V_{\max}/V_{pl}\right)} \tag{22}$$

A finer estimate of $\theta_i(x)$ might matter at very long propagation distances, where V_{prop} is underestimated because the positive stressing rate ahead of the rupture front tends to decrease θ. However, slip rate is insignificant in the long-distance range.

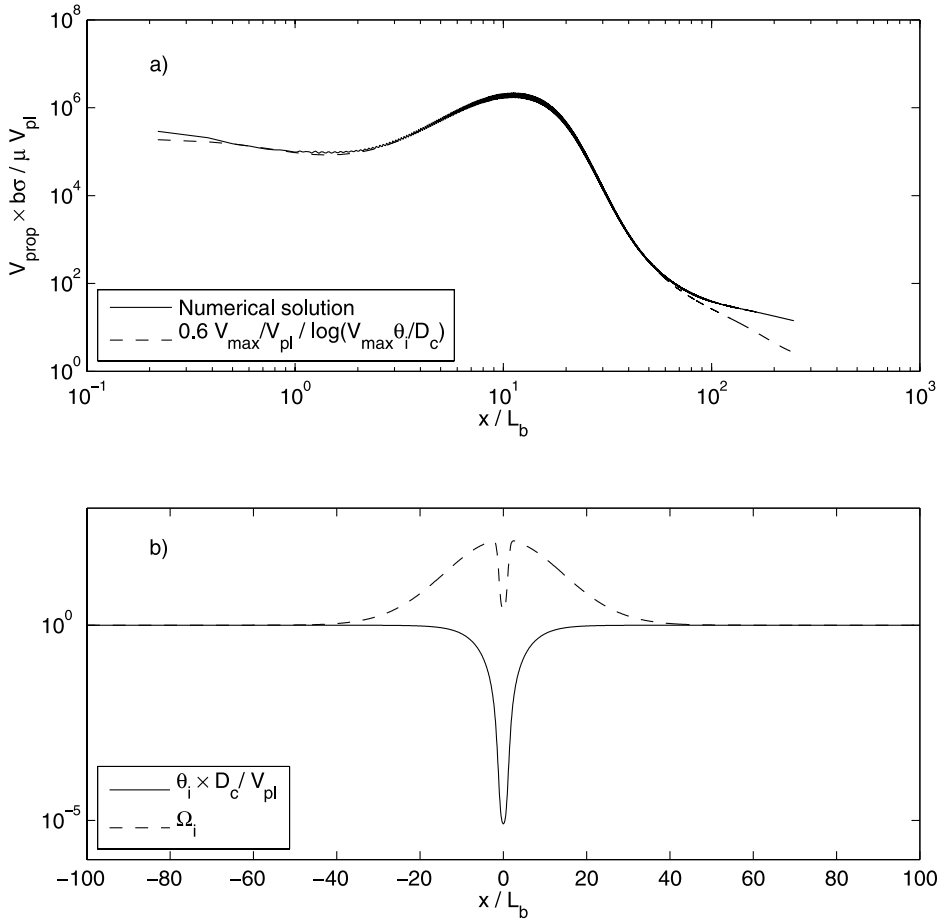

Figure 3. (a) Crack propagation speed V_{prop} on a strengthening fault from the example in Figure 2 (solid curve) compared to relation 39 (dashed curve) with θ_i taken from the snapshot below. (b) Spatial distribution of state variable θ (solid curve) and $\Omega = \theta V/d_c$ (dashed curve) at the onset of crack propagation.

[31] Figure 4 summarizes some properties of transients triggered on a 2-D model with patch size $L = 30\ L_b$ and $b/a = 0.9$, as a function of the length scale R_0 and the amplitude $\Delta\tau_0$ of the initial shear stress perturbation. The peak value of $V_{\max}(t)$ increases with the amplitude of the perturbation $\Delta\tau_0$ (Figure 4, left). The time to instability $t_{\max}$, defined as the time needed to reach the peak velocity, decreases with increasing $\Delta\tau_0$ and vanishes for sufficiently small R_0 (Figure 4, center). For a given size of the perturbation, the maximum velocity increases with the amplitude of the perturbation (Figure 4, right). For the aging law (Figure 4, top), the overall dependence of $V_{\max}$ and $t_{\max}$ on the initial conditions is well captured by the following asymptotic behaviors:

[32] 1. Very wide initial perturbations ($R_0 \gg L$, solid curve) result in almost uniform slip. The peak velocity and its timing can be obtained from a 1-D model in the self-accelerating approximation ($\Omega \gg 1$), as given by equations (B16) and (B17):

$$V_{\max} \approx V_{pl} \exp[\Delta\tau/(a-b)\sigma] \tag{23}$$

$$t_{\max} \approx \frac{a}{b}\frac{d_c}{V_{pl}} \exp(-\Delta\tau/a\sigma) \tag{24}$$

This asymptotic regime is indicated by solid curves. Equation (B6) captures the monotonic decay of $t_{\max}$ as a function of $\Delta\tau_0$. The slight underestimation of $t_{\max}$ and overestimation of $V_{\max}$, even in the limit of very large R_0, is due to our approximate usage of the solutions from the self-accelerating regime, $\Omega \gg 1$, up to the return to steady state conditions, $\Omega \approx 1$ (Appendix B2).

[33] 2. For very narrow initial perturbations ($R_0 \gg L_b$), slip decelerates monotonically toward V_{pl}, without acceleration transient, as would happen on a very stiff 1-D model with $K \gg K_b$. The peak velocity is reached at $t_{\max} = 0$ and is given by the initial velocity V^+ obtained from equation (5):

$$V^+ = V_{pl} \exp\left(\frac{\Delta\tau_0}{a\sigma}\right). \tag{25}$$

This asymptotic regime is indicated by dashed curves in Figure 4 (left), and the corresponding simulations (with $t_{\max} = 0$) are not shown in Figure 4 (right).

[34] 3. Seismic events appear when dynamic effects become significant, above a threshold slip velocity of order

$$V_{dyn} = \frac{2a\sigma c_s}{G} \tag{26}$$

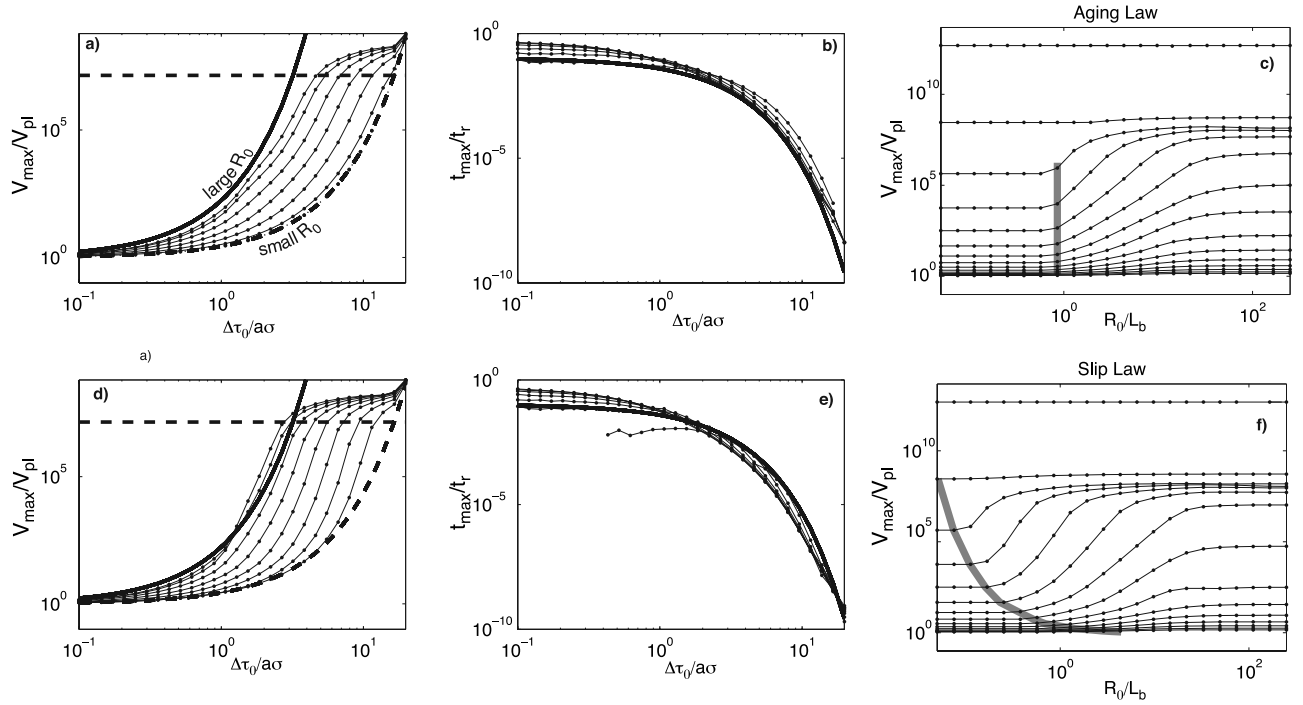

Figure 4. Properties of transients triggered by a positive shear stress step on a strengthening fault patch of size $L = 30\ L_b$ with $b/a = 0.9$ under (top) the aging law or (bottom) the slip law. (left) Peak slip velocity $V_{\max}$ normalized by the secular slip velocity V_{pl} and (middle) time to peak velocity $t_{\max}$ normalized by the characteristic relaxation time t_r are plotted as a function of the amplitude of the stress perturbation $\Delta\tau_0$ for various values of the perturbation length scale $R_0 = (1.5)^n\ L_b/20$ with $n = 0$ to 21 (the largest value is $R_0 \approx 250\ L_b$). (right) The peak velocity as a function of R_0 is also plotted for a given amplitude of the perturbation, the thick grey lines showing the size of the perturbation for which $V_{\max}$ exceeds by at least 10% its value at the minimum radius.

that arises from the competition between radiation damping and the direct effect of rate-and-state friction [*Rubin and Ampuero*, 2005]. This limit is indicated by a horizontal dashed line in Figure 4 (left). The condition for quasi-static motion, $V \gg V_{dyn}$, is valid when $\Omega \gg 1$ and, as shown by *Ampuero and Rubin* [2008], is more stringent than the condition $V_{prop} \gg c_s$. Dynamic (seismic) slip velocities are reached for perturbation amplitudes $\Delta\tau_0 \gg a\sigma$, and require lower $\Delta\tau_0$ at larger R_0.

[35] Perturbations of radius larger than the nucleation length L_b induce acceleration transients. In the intermediate regime, $L_b < R_0 < L$, the 1-D approximation is inappropriate because relaxation occurs over a zone of variable size (variable stiffness).

[36] Figure 4 also allows comparisons between the aging law (top) and the slip law (bottom). Both state evolution laws predict large slip rates if $\Delta\tau_0 \gg a\sigma$. The response of a fault governed by the aging law is stronger if the size R_0 of the perturbation is larger than the nucleation size L_b (grey thick line in Figure 4c), due to the emergence of acceleration transients. For the slip law, this transition occurs at smaller R_0 for larger $\Delta\ \tau_0$ (thick grey line in Figure 4f). The transition size corresponds closely to L_b' given by equation (20) with $\theta_i \approx d_c/V_{pl}$,

$$L_b' \approx L_b \left(\ln \frac{V_{\max}}{V_{pl}} \right)^{-1}. \tag{27}$$

In the large wavelength limit, $L \gg L_b$, this becomes

$$L_b' \approx L_b \frac{(a-b)\sigma}{\Delta\tau_0} \tag{28}$$

after use of equation (B17) and (27). When $a \approx b$, the nucleation length of the slip law becomes very small. However, it cannot reach arbitrarily small values because dynamic effects (that become significant when $V \gtrsim V_{dyn}$) limit the peak velocity. In summary, both evolution laws show significant acceleration when the radius of the perturbation is larger than the nucleation length (L_b for the aging law and L_b' for the slip law).

[37] The slip law has a higher potential for instability. It yields (nearly one order of magnitude) larger peak velocities than the aging law and generates acceleration transients even for narrow perturbations ($R_0 < L_b$) with sufficiently large amplitude (for large $\Delta\tau_0$ all curves depart from equation (3)). These differences are expected from 1-D nonlinear stability analysis [*Gu et al.*, 1984; *Ranjith and Rice*, 1999] showing that the slip law is generally more unstable than the aging law and is only conditionally stable when $K > K_c$. These differences are also related to a smaller localization size and a narrower crack process zone in the case of the slip law, analogous to the results on weakening faults of *Ampuero and Rubin* [2008]. The time to instability (Figure 4, bottom right) agrees with the estimate derived for the aging law, equation (B6).

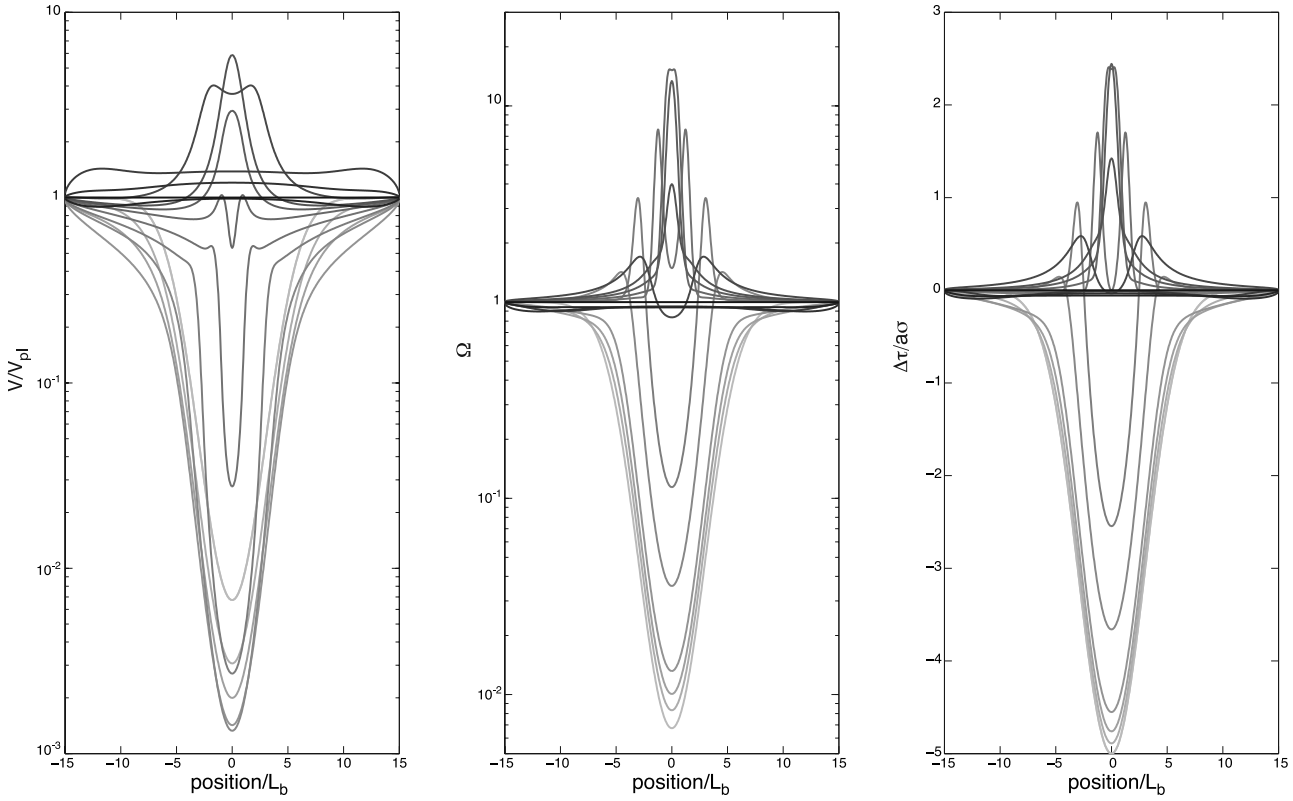

Figure 5. From left to right are shown profiles of velocity, Ω, and stress change at various times, in response to a shear stress change of radius $R_0 = 3\ L_b$ and amplitude $\Delta\tau_0 = -5a\sigma$. Lighter curves are snapshots at earlier times. The 2-D fault has a width $L = 30\ L_b$ and is governed by the aging law with $b/a = 0.9$. Each profile correspond to an increase of 15% of the mean velocity. The heavy line represents the variable immediately after the onset of the perturbation.

[38] The peak propagation speed of the transient can be estimated by combining equations (22) and (23):

$$V_{prop} \approx V_{pl} \exp\left(\frac{\Delta\tau}{(a-b)\sigma}\right) \frac{G}{\Delta\tau} \frac{a-b}{b} \tag{29}$$

The exponential term gives a very strong dependence on the amplitude $\Delta\tau$ of the stress trigger. The susceptibility is stronger at high fluid pressure, low effective normal stress σ, or near the transition zone where $a \approx b$. This estimate is quasi-static and breaks down when $V_{\max} \approx V_{dyn}$ (defined in equation (26)), that is when

$$\Delta\tau \approx (a-b)\sigma\ \ln\left(2ac_S\sigma/GV_{pl}\right) \tag{30}$$

At that point the propagation speed is

$$V_{prop} \approx 2\frac{a}{b}c_S/\ln\left(2a\sigma c_S/GV_{pl}\right) \tag{31}$$

For reasonable parameter values this gives $V_{prop}/c_s \approx 1/20$, which is much higher than the average propagation speeds of postseismic, episodic slow slip and tremor swarms. However, this is of the same order as the typical speed of the so-called slow rupture fronts observed in laboratory experiments of dynamic rupture [*Rubinstein et al.*, 2004].

4.2. Response to Negative Coulomb Stress Perturbations

[39] So far, we have been only concerned by static positive perturbations of the Coulomb stress, that is perturbations that instantaneously increase the sliding velocity of the creeping fault. We now consider the case of perturbations that decrease the static Coulomb stress and will show that they may also cause acceleration transients.

[40] We consider again the 2-D model of fault patch of section 4.1 (size $L = 30\ L_b$ and $b/a = 0.9$). Figures 5 and 6 show, for the aging law and for the slip law, respectively, the spatial distribution of the sliding velocity V, the "distance to steady state" Ω, and the incremental stress $\Delta\tau$ at various times after an initial shear stress perturbation of characteristic length $R_0 = 3L_b$ and peak amplitude $\Delta\tau_0 = -5\ a\sigma$. The creep episode can be divided into four consecutive phases: (1) initial deceleration; (2) acceleration back to $\approx V_{pl}$, starting from the edges of the initial perturbation and propagating towards the center, analogous to a pair of converging quasi-static crack fronts; (3) coalescence of the two fronts and slip acceleration over a zone of size $\approx L_b$ until reaching a peak slip velocity; and (4) lateral propagation of two (smeared) crack-like fronts with overall relaxation back to steady state.

[41] The first stage can be understood from a 1-D model, developed in Appendix B3. In particular, when $R_0 > L_b$, the

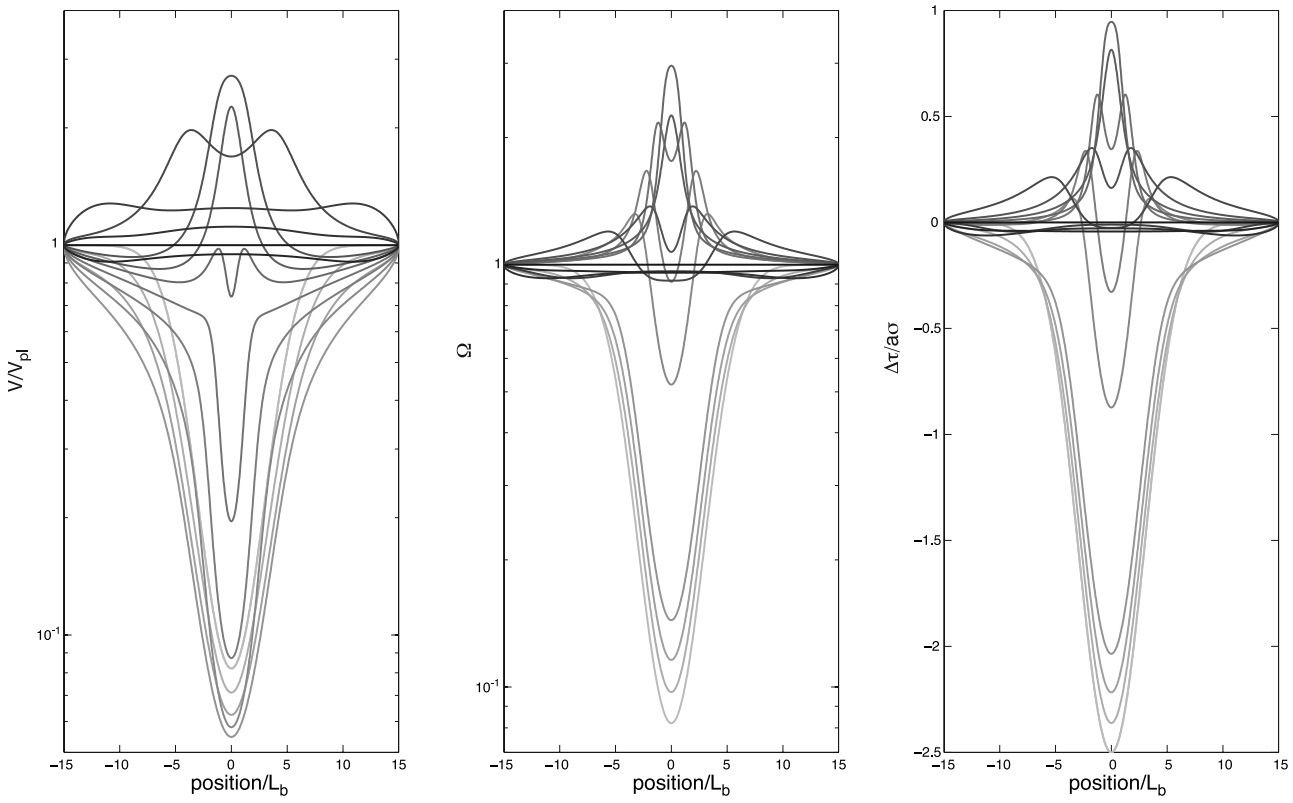

Figure 6. Same as Figure 5 for the slip law with a perturbation of radius $R_0 = 3\ L_b$ km and amplitude $\Delta\tau_0 = -2.5\ a\sigma$.

timescale for initial deceleration is of the order of (see equation (B23) with $K_b/K \approx R_0/L_b$)

$$t_1 = \frac{d_c}{V_{pl}} \left(\frac{R_0}{L_b} - 1 \right) . \tag{32}$$

[42] During the second stage, the two converging fronts induce a local increase of the stressing rate at the center of the fault patch that can be large enough for Ω to increase significantly above 1 (up to 20 in the aging law example of Figure 5b and above 2 in the slip law example of Figure 6b). This excursion above steady state promotes a slip acceleration transient (stage 3). The subsequent evolution (stages 3 and 4) is analogous to the development of a transient episode in the case of positive Coulomb stress perturbations (section 4.1). However, the fault can not be considered as evolving in the self-accelerating phase since $\Omega \gg 1$ is not strictly verified. This makes the case $\Delta\tau_0 < 0$ much more difficult to deal with from an analytical point of view. We will nevertheless present an estimate of the time to instability $t_{\max}$ which agrees with the numerical results.

[43] Figure 7 shows the amplitude $V_{\max}$ (left) and timing $t_{\max}$ (center) of slip transients induced by a negative shear stress perturbation as a function of its radius R_0 and amplitude $\Delta\tau_0$, for the aging law (Figure 7, top) and for the slip law (Figure 7, bottom). Figure 7 (right) shows the peak velocity as a function of the radius of the perturbation of fixed amplitude $\Delta\tau_0$. For both state evolution laws the peak velocity $V_{\max}$ increases with the radius of the perturbation. For a given radius, $V_{\max}$ first increases as a function of $|\Delta\tau_0|$ but then decreases. In the case of the aging law, the strongest response is observed for $\Delta\tau_0 \approx -8a\sigma$, a crossover value that does not depend on R_0. Peak velocities of the order of $V_{\max} \approx 80\ V_{pl}$ can be observed if the whole creeping fault is perturbed ($R_0 \gg L$). The slip law shows similar behavior, with maximum response at $\Delta\tau_0 \approx -2.5\ a\sigma$, but the peak $V_{\max}$ is almost one order of magnitude lower than for the aging law.

[44] The fact that in these 2-D models the peak sliding velocity does not depend monotonically on the amplitude of the perturbation is a major difference with the predictions of a 1-D model (see Appendix B3 and Figure B1). In a multidimensional model the fault is affected by two competing effects. On one hand $V_{\max}$ tends to increase with $|\Delta\tau_0|$ just as in the 1-D case (Appendix B3). On the other hand, the stressing rate induced by the converging slip fronts (Figure 5) increases with their propagation speed V_{prop}, which in turn decreases with $|\Delta\tau_0|$ as shown by equation (33). Hence the stressing rate that drives the transient acceleration tends to decrease with the amplitude of the initial perturbation. The maximum in the fault response reflects a compromise between these two competing processes, the second of which cannot be captured by a 1-D model.

[45] The time to instability $t_{\max}$ increases monotonically with $|\Delta\tau_0|$ and does not depend strongly on the choice of the state evolution law. Unlike the case $\Delta\tau_0 > 0$, $t_{\max}$ is systematically larger than t_r when $\Delta\tau_0 < 0$, and the creep transient can occur long after the onset of the perturbation. Peak velocity is reached upon coalescence of the converging fronts nucleated at the edge of the initial stress drop

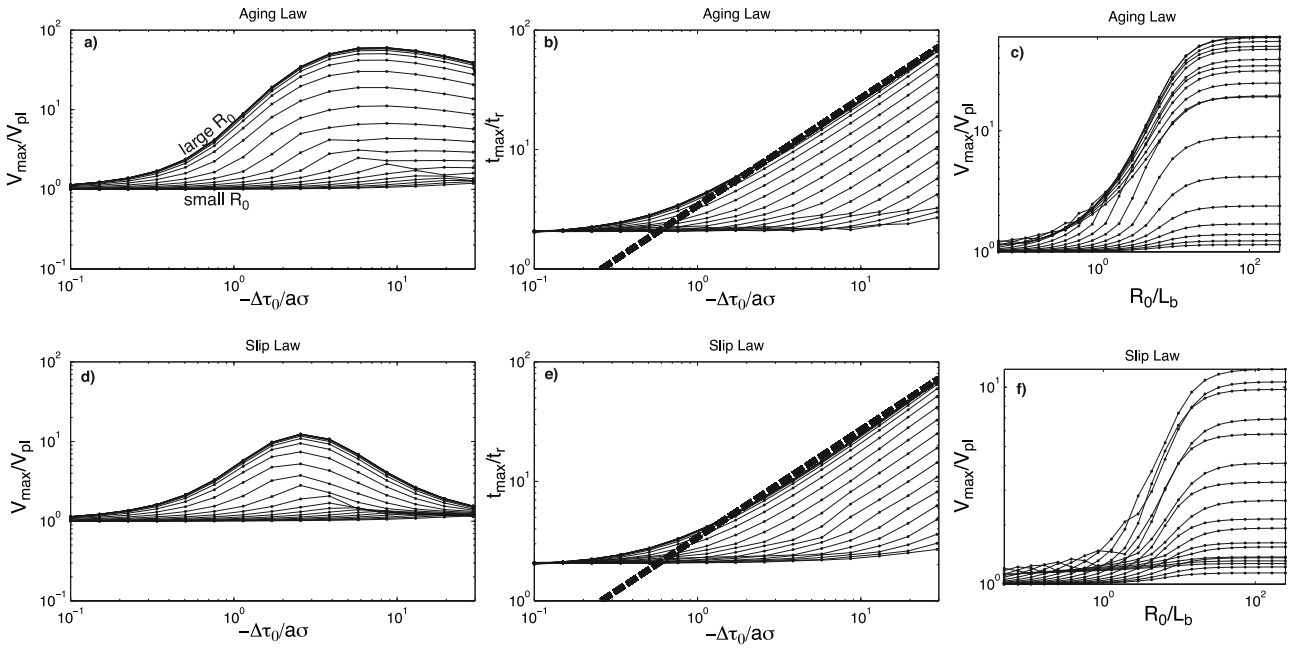

Figure 7. Same as Figure 4, but considering the response of the strengthening fault patch to negative shear stress steps ($\Delta\tau_0 < 0$). The thick dashed lines on the center plots show the time to instability predicted by equation (34).

region. Their propagation speed V_{prop} can be estimated from equation (39) by taking $V_{\max} = V_{pl}$ (the slip velocity scale at and behind the fronts) and $\theta_i = d_c/V^+$, where the initial velocity V^+ is given by equation (3). This yields

$$V_{prop} \approx V_{pl}\,\frac{G}{b\sigma}\,\frac{a\sigma}{-\Delta\tau_0}. \tag{33}$$

The time $t_{\max}$ at which the two fronts merge can be estimated as the propagation time over a distance R_0 at speed V_{prop}:

$$t_{\max} \approx \frac{R_0}{V_{prop}} = \frac{R_0}{G}\,\frac{b}{a}\,\frac{-\Delta\tau_0}{V_{pl}}. \tag{34}$$

If $R_0 > L$ the propagation distance of the converging cracks is instead L, and in the expression above R_0 should be replaced by L. Interpreting the first term on the right hand side as the inverse of the stiffness K of a slip region of characteristic size R_0 (or L), equation (34) is equivalent to the 1-D result of equation (B26). It is rather surprising that the timing of the 2-D instability, which arises from the coalescence of propagating fronts, remains so close to the result of a 1-D model where propagation is ignored.

[46] Unlike the case of positive steps in Coulomb stress, the slip and aging law show similar behavior for a perturbation of fixed amplitude but variable size (Figure 7, right): An increased acceleration is observed when the size of the perturbation becomes roughly larger than L_b. This is not surprising noting that the contraction factor $L_b'/L_b \approx 1/\ln(V_{\max}/V_{pl})$ for the localization length of the slip law is at most ≈ 3 since $V_{\max}/V_{pl} \lesssim 20$, so that it may be roughly considered that the nucleation length of the slip law is independent of the amplitude of the negative stress step.

4.3. Summary of Useful Relationships

[47] We summarize here the most important analytical expressions that may be used to quantify the response of a strengthening fault to step perturbations of Coulomb stress. Most of these expressions are greatly simplified in the large wavelength limit, i.e., when the shortest characteristic size L of the strengthening fault region (usually its downdip extension) and the perturbation length scale R_0 are much greater than the localization length given by

$$L_b = \frac{Gd_c}{b\sigma} \quad \text{for the aging law,} \tag{35}$$

or

$$L_b' = \frac{Gd_c}{b\sigma}\left(\ln\frac{V_{\max}}{V_{pl}}\right)^{-1} \quad \text{for the slip law,} \tag{36}$$

where $V_{\max}$ is the maximum slip velocity.

[48] Positive Coulomb stress perturbations, $\Delta\tau_0 > 0$, of length scale R_0 larger than the localization length (L_b or L_b') generate slip acceleration transients with duration and peak velocity given by

$$t_{\max} \approx \frac{a}{b}\,\frac{d_c}{V_{pl}}\exp\left(-\frac{\Delta\tau_0}{a\sigma}\right),\ R_0 \gg L_b \tag{37}$$

and

$$V_{\max} \approx V_{pl}\exp\left(\frac{\Delta\tau_0}{(a-b)\sigma}\right),\ R_0 \gg L_b, \tag{38}$$

respectively. The propagation velocity V_{prop} of a slip front in a velocity strengthening region originally creeping at the

long term velocity V_{pl} is related to the peak slip velocity $V_{\max}$ at the rupture front by

$$V_{prop} \approx V_{\max} \frac{G}{b\sigma} \left(\ln \frac{V_{\max}}{V_{pl}} \right)^{-1}. \quad (39)$$

[see *Ampuero and Rubin*, 2008, equation (53)]. In the case of a negative step in Coulomb stress, the time to peak slip velocity is

$$t_{\max} \approx -\frac{b}{a} \frac{R_0 \Delta\tau_0}{G V_{pl}}, \quad (40)$$

and the propagation velocity is

$$V_{prop} \approx V_{pl} \frac{G}{b\sigma} \times \frac{a\sigma}{-\Delta\tau_0}, \quad (41)$$

5. Discussion

5.1. Possible Origins of the Perturbations

[49] In this work, we have studied the response of a creeping fault to a sudden change in Coulomb stress induced by an external perturbation. We discuss here the possible origins of such perturbations.

[50] Postseismic slip is unambiguously triggered by the coseismic stress changes induced by the main shock. An earthquake induces significant stress changes over an area of size comparable to the rupture size. Since significant postseismic slip is only observed following large earthquakes, that rupture the whole thickness of the seismogenic zone, postseismic slip corresponds to large scale (>10 km) stress changes.

[51] Slow slip events, such as those observed in the Cascadia subduction zone, seem to be induced by stress perturbations of much smaller wavelengths. J.-P. Ampuero and H. Perfettini (manuscript in preparation, 2008) discuss the triggering of creep events by brittle asperities present in the creeping region. Nevertheless, this mechanism is difficult to reconcile with the existence of the seismic tremors related to slow slip events [*Obara*, 2002; *Rogers and Dragert*, 2003; *Obara et al.*, 2004; *Kao et al.*, 2005]. A more complete model should incorporate variables such as porosity and pore pressure, together with an evolution law relating porosity and creep rate. Although such modeling is beyond the scope of the present article, we outline next some basic ideas.

[52] Volcanic tremors are usually interpreted as due to the circulation of fluids [*Chouet*, 1992; *Ferrazzini and Aki*, 1992]. The nonvolcanic tremors connected to slow earthquake have been sometimes attributed to metamorphic dehydration reactions. Fluids are released by metamorphic reactions over a broad range of depths. Part of those fluids migrate updip the subduction interface, channeled by the fault zone itself, until they encounter less permeable materials. In the fault valve model proposed by *Sibson* [1992], ductile creep within mostly sealed fault zones compacts the fault gouge and increases fluid pressure [*Sleep*, 1995], until the reduction of the effective normal stress is large enough for the accumulated shear stress to counteract the frictional resistance. Then slip occurs and changes the mechanical state of the fault from undrained to drained, resulting in an increase of the porosity. After the slip episode the fault zone starts to compact again for another cycle. Such a mechanism has been advocated to explain the cyclic behavior of events in the seismogenic zone [*Sleep and Blanpied*, 1992; *Sleep*, 1995].

[53] Because ductile creep is even more active in the transition zone, due to higher temperatures, the fault valve mechanism seems even more likely in this part of the fault and is consistent with the generation of seismic tremors by the expulsion of fluids away from the fault zone. This fluid release would induce a drop in pore pressure and a negative Coulomb stress perturbation that may be sufficient to generate a transient creep episode such as those studied in section 4.2. The propagation of the slow earthquake would increase the creep rate along its way, increasing the compaction rate, and eventually trigger secondary creep instabilities in areas where the shear stress was already close to the frictional stress.

5.2. Estimate of the Size and Time to Instability for Natural Cases

[54] In order to discuss the relevance of our results for real faulting, it is necessary to bound the parameters $t_{\max}$ and L_b. There are large uncertainties about the appropriate value of d_c, which ranges from 1 μm to 1 cm in laboratory experiments [*Marone*, 1998]. Assuming $a \approx b$ and taking typical laboratory values $a = 10^{-3}-10^{-2}$ [*Marone*, 1998], and effective normal stress $\sigma \approx 100$ MPa, or the range $a\sigma = 0.1-1$ MPa inferred from aftershock and postseismic observations, yields rather small localization length scales $L_b = 3$ cm to 3 km. Large earthquakes induce large-scale (several tens of kilometers) stress perturbations. This suggest that the large-scale limit ($L \gg L_b$) applies.

[55] At the top of the transition zone, where $a \approx b$, the time to instability in response to a positive Coulomb stress step is $t_{\max} \approx d_c/V^+$ (from equation (B17)), where the sliding velocity V^+ immediately after the stress step may vary from typical postseismic values (e.g., 10^3 V_{pl} as discussed by *Perfettini and Avouac* [2004] and *Perfettini et al.* [2005]) to seismic rupture velocities (1 m/s). Therefore $t_{\max}$ may span an enormous range of short timescales, from 10^{-6} s to 2 days. At the lower end of this range, slip acceleration would be too short to be considered as postseismic slip and would rather qualify as part of the main shock or as an early aftershock. At the higher end, the detection of short acceleration transients still requires high-quality, high sampling rate geodetic data. Recent analysis of the postseismic slip of the 2004 Parkfield earthquake by *Langbein et al.* [2006], consistent with a velocity-strengthening rheology except in the first hour of relaxation [see, e.g., *Langbein et al.*, 2006, Figure 3], suggests values of $t_{\max}$ shorter than one hour. An earthquake catalog of the Chi-Chi aftershocks obtained from accelerometric records [*Chang et al.*, 2007] shows that the seismicity rate decays monotonically as 1/time, starting as early as 2–3 mn after the main shock (J.-P. Avouac, personal communication, 2008), suggesting a value of $t_{\max}$ lower than 2 mn.

[56] Large earthquakes can induce slip transients, as was the case for the 23 June 2001 Arequipa (M_w 8.4), Peru, earthquake [*Melbourne and Webb*, 2002]. Its largest after-

shock, the 7 July (M_w 7.6) event, was preceded by 18 h by an aseismic transient consistent with slip acceleration (about 2 cm in 18 h) in the downdip vicinity of the 7 July hypocenter, presumably at the top of the transition zone [*Melbourne and Webb*, 2002]. The postseismic phase of the 30 July 1995 (M_w 8.1) Antofagasta, Chile, earthquake presents a similar case. *Pritchard and Simons* [2006a] observed the growth of an aseismic slip pulse at the downdip termination of the main shock coseismic slip, starting in November 1996 and lasting 1 year. The transient may have triggered the M_w7.1 earthquake on 30 January 1998. In these two examples, the time delay between the main shock and the transient peak velocity ranges from 2 weeks to 2 years. These slip transients could be either due to an increase or a decrease in Coulomb stress. We now examine those two scenarios.

[57] The observed delay times are much longer than our previous estimates of $t_{\max}$ for positive Coulomb stress steps (10^{-6} s to 2 days). Since $t_{\max} \approx d_c/V^+$ at the top of the transition zone, then either d_c is at least metric or V^+ is much smaller. The latter is not an option because the initial velocity needs to be significant ($V^+ \gtrsim 100\ V_{pl}$) in order for the transient to be detectable. Values of d_c of the order of one meter are much larger than laboratory values. However, there is a notorious lack of laboratory experiments at pressure and temperature conditions relevant for the top of the transition zone. If d_c scales with fault zone width or with cumulative slip [*Marone and Kilgore*, 1993], it may reach larger values than commonly thought in the transition zone, due to the many tens of kilometers of slip accumulated during subduction. Still, for an exhumed mature section of the San Andreas fault, *Marone and Kilgore* [1993] proposes values of d_c that are only millimetric. Moreover, values of $d_c \gtrsim 1$ m imply huge localization lengths (L_b or L_b') inconsistent with the spatial extent of the creep pulse mentioned by *Pritchard and Simons* [2006a]. Hence, triggering of these slip transients by an increase of Coulomb stress is an unlikely scenario.

[58] If the transients were initiated by a decrease in Coulomb stress, then we have to identify a possible cause for such a perturbation. The main shock itself can not generate directly a negative step in Coulomb stress, but it might do so indirectly by inducing secondary processes. Among them is the breakage of isolated fluid pockets. If prior to the main shock the fault was undrained, then some areas might have been overpressured. The main shock rupture may have broken some of those pockets, allowing the pressurized fluids to escape rapidly. This would result in fault clamping, a rapid increase in effective normal stress from a value near 0 to a value close to the lithostatic pressure. According to the results of section 4.2, a slip transient will follow long after the main shock. The stronger the drop in fluid pressure the longer the delay time, plausibly as large as 2 weeks or 2 years.

[59] Among the two speculative scenarios considered above, only clamping of the fault due to the breakage of overpressured fluid pockets induced by seismic rupture is consistent with the observations of *Melbourne and Webb* [2002] and *Pritchard and Simons* [2006a]. Similar examples might soon become quite common with the increase of dense continuous GPS network observations.

[60] Slip acceleration transients, such as frictional afterslip or slow slip transients, significantly increase the loading rate on their vicinity, decreasing the recurrence time of the nearby locked patches. If a brittle area of the fault is already at the end of its earthquake cycle, the occurrence of such events is very likely to trigger them. Postseismic slip can trigger earthquakes as in the case of 1994 Sanriku-haruka-oki, Japan, earthquake (M_w7.7) [*Yagi et al.*, 2003]. The largest aftershock of this event, a M_w6.9 earthquake, occurred 10 d later, and its hypocenter was located on the edge of the postseismic patch. *Yagi et al.* [2003] mention an initial phase of slip acceleration up to 30 mm/day during the period preceding the M_w6.9 event. It is likely that this aftershock occurred in a region already preloaded by the main shock, the reloading by the nearby afterslip (which locally increases the loading rate by many orders of magnitude) bringing it to failure.

5.3. Equivalence Between Pure Velocity-Strengthening and Complete Rate-and-State Formulations During Postseismic Slip

[61] Numerous studies have shown that postseismic deformation is consistent with slip on portions of the fault with pure velocity strengthening friction [*Marone et al.*, 1991; *Hearn et al.*, 2002; *Perfettini and Avouac*, 2004; *Perfettini et al.*, 2005; *Hsu et al.*, 2006; *Perfettini and Avouac*, 2007]:

$$\mu = \mu^* + a' \ln\left(\frac{V}{V^*}\right) \tag{42}$$

with $a' > 0$. It is clear from equations (8) and (42) that pure velocity strengthening friction is equivalent to rate-and-state friction at steady state with parameters a and b such that $a' = a - b$. However it is not immediately obvious under which circumstances the steady state assumption is a good approximation of the complete rate-and-state fault response.

[62] In a spring block (1-D model) with pure velocity-strengthening friction, initially sliding at steady state, the slip velocity in response to a step in shear stress decreases monotonically as [*Perfettini et al.*, 2005]

$$V(t) = \frac{V^+\ e^{t/t_r}}{1 + \dfrac{V^+}{V_{pl}}\left(e^{t/t_r} - 1\right)} \tag{43}$$

with decay time t_r and initial velocity V^+ given by equations (B5) and (3), respectively, changing a by a'. In the complete rate-and-state case we have shown in section and in Appendix B1 that a fault of size $L \gg L_b$ responds instead by an initial acceleration up to maximum velocity $V_{\max}$, over a timescale $t_{\max}$, and then relaxes in steady state. The slip evolution during the relaxation stage, given in equation (B20), is exactly the same as in equation (43) after obvious parameter identifications are made ($V^+ = V_{\max}$ and $a' = a - b$).

[63] In practice, the timescale $t_{\max}$ of the acceleration transient is short (at most a few days as discussed in section 5.2) compared to the characteristic duration t_r of postseismic slip (typically a few years). The correspondence between the pure velocity-strengthening and the complete rate-and-state rheologies is warranted during most of the postseismic period if $L \gg L_b$.

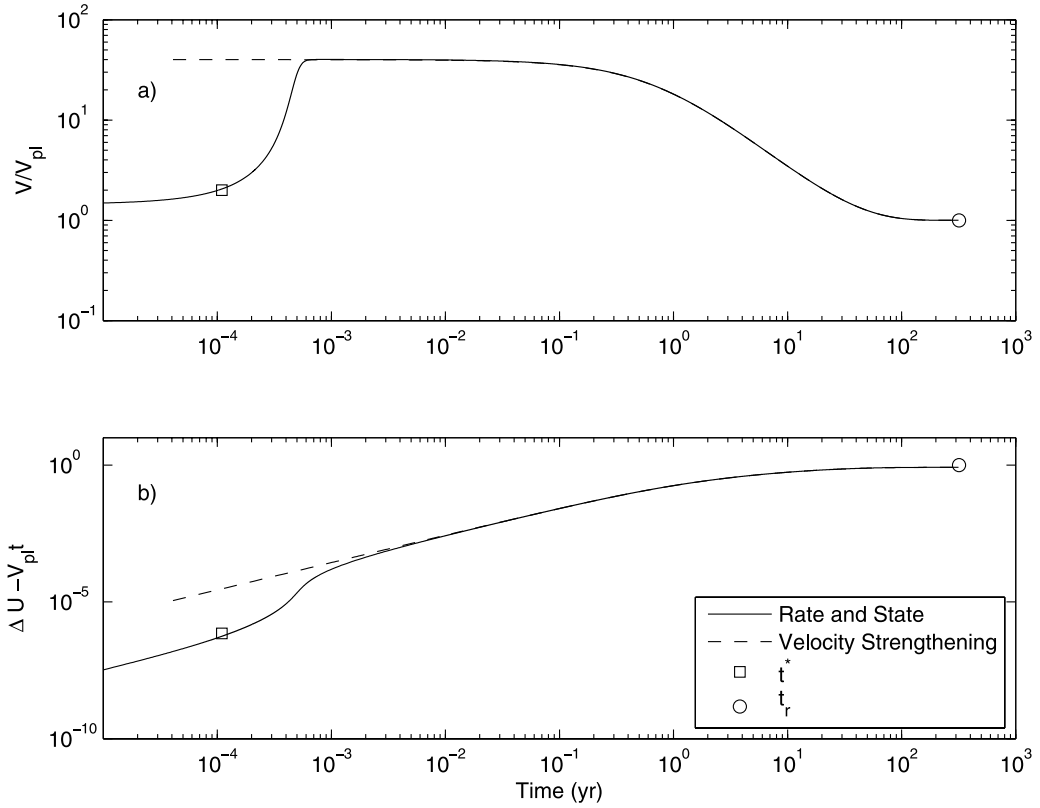

Figure 8. (a) Velocity of a spring slider system in response to an initial step in velocity. Both the RS (continuous line) and VS (dashed line) are considered. After a transient phase, in the RS case, where the velocity increases, both rheologies lead to the same prediction, providing that the parameters of both models are chosen adequately as discussed in the main text. (b) Same as Figure 8a for displacement.

[64] As an example we consider the postseismic phase of the 1992 Landers earthquake. Modeling this event under pure velocity-strengthening friction, *Perfettini and Avouac* [2007] inferred $a'\sigma \approx 0.5$ MPa. Assuming $L = 30$ km, $V_{pl} = 7$ mm a^{-1}, $b/a = 0.9$, $d_c = 10^{-6}$ m, and $V_{\max} = 40\ V_{pl}$ implies $L_b \approx 7$ mm, $t_{\max} \approx 10^{-4}$ year (less than 1 day), and $t_r' \approx 23$ year. As $L \gg L_b$ and $t_{\max} \ll t_r$, the correspondence between the two approaches is justified. The two predictions are virtually identical from $t_{\max}$ to the end of the relaxation phase (Figure 8). Both formalisms strongly differ in the initial slip rate V^+ they require to achieve a given peak slip rate $V_{\max}$. Because it exhibits a strong spontaneous acceleration phase, the rate-and-state model needs a much lower initial velocity than the velocity-strengthening model: $V^+/V_{pl} = \exp(\Delta\tau/a\sigma) = 1.45$ in the former and $V^+/V_{pl} = \exp[\Delta\tau/(a-b)\sigma] = 40$ in the latter. This difference is accentuated at the transition zone, where $a \approx b$.

[65] The correspondence between velocity-strengthening and rate-and-state is more difficult to evidence in a multidimensional model because the limit $L \gg L_b$ is hard to achieve while maintaining proper numerical resolution ($\Delta x \ll L_b$). The example shown in Figure 9 corresponds to $V_{pl} = 45$ mm a^{-1}, $a\sigma = 1$ MPa, $b/a = 0.9$, $d_c = 10^{-3}$ m. These values yield $L_b \approx 33$ m and $t_{\max} \approx 6$ days. Initial conditions are the same as in the previous 1-D example. Again, the agreement between the two approaches is quite good after $t_{\max}$. However, now the initial velocity in the velocity-strengthening case is not equal but higher than the maximum velocity $V_{\max}$ of the rate-and-state transient, a difference that might disappear for a large enough ratio L/L_b (but we were unable to confirm this due to numerical constraints).

[66] During steady state relaxation, equation (43) shows that the velocity decays roughly as $1/t$. If L is not much larger than L_b steady state does not prevail in the early stage of relaxation ($t \gtrsim t_{\max}$) and slip decays as $1/t^p$, where p is an exponent that may differ significantly from the value $p = 1$ (see for instance phases 4–5 of Figure 1). Possible heterogeneities of frictional parameters can complicate further this picture. The sometimes observed deviation of estimated p values from $p = 1$ does not rule out the rate-and-state hypothesis.

5.4. Nature of Superficial Afterslip

[67] Even though most of the afterslip following large earthquakes usually occurs below the base of the seismogenic zone, shallower afterslip, at depths generally considered seismogenic, has also been widely documented [*Marone et al.*, 1991; *Hsu et al.*, 2006]. A fundamental question is whether this superficial afterslip is related to the relaxation of velocity strengthening regions or to the relaxation of stable velocity weakening regions.

[68] The first scenario seems to apply in the case of the 2005, M_w8.7, Nias earthquake. *Hsu et al.* [2006] have shown inverting GPS data that most of the afterslip following this event was superficial and was located updip of the

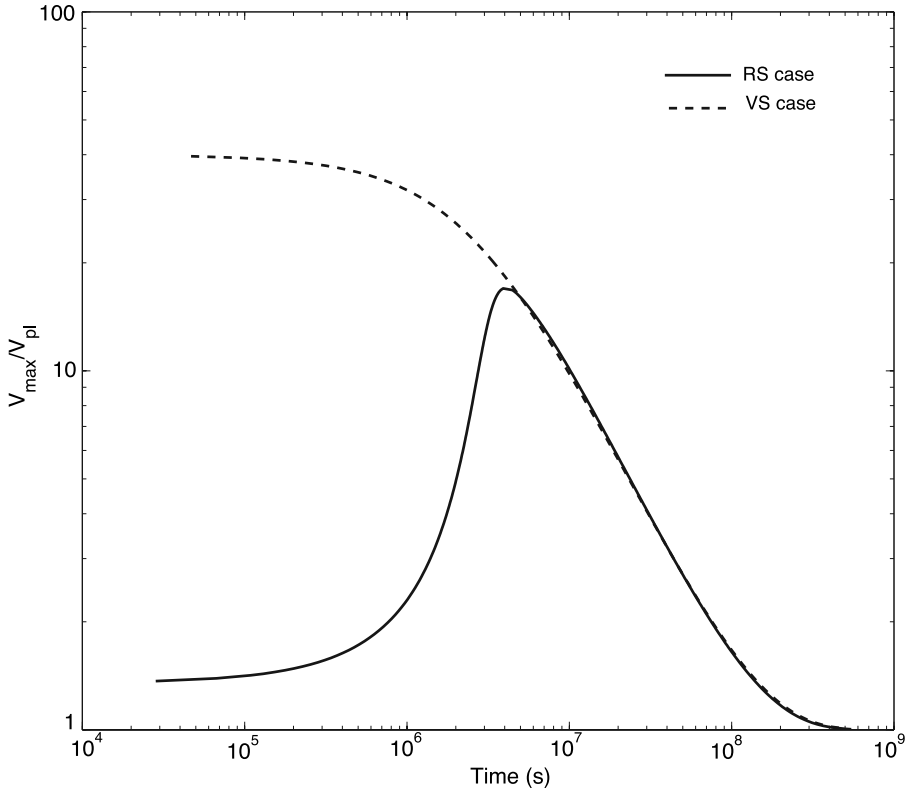

Figure 9. Same as Figure 8 for the 2-D fault model. See main text for details.

main coseismic asperities. *Chlieh et al.* [2008] have shown, considering geodetic and paleogeodetic measurements, that the areas of large coseismic slip of the Nias earthquake were apparently locked during the interseismic period, while the zones of significant afterslip were creeping between large subduction events. Consequently, the velocity strengthening and weakening regions on the Sumatra megathrust seem to be related to permanent frictional properties.

[69] A velocity weakening region responds to the high stress changes (implying $\Omega \gg 1$) induced by a nearby main shock rupture with an aseismic slip transient, consistent with superficial afterslip, only if its shortest dimension L is smaller than L_b. Otherwise the fault region accelerates to dynamic rupture which, depending on the triggering timescale, can be interpreted as a composite subevent inside the main shock or as an aftershock. Alternatively, a velocity weakening region with $L > L_b$ can exhibit postseismic relaxation if the main shock induces a large reduction of the effective normal stress that increases L_b beyond L, stabilizing the region. This scenario is reasonable only if L is of the same order as the initial L_b, otherwise it requires an almost complete drop in effective normal stress. In any case, the velocity weakening regions that can generate postseismic slip need to have a characteristic size at most of the order of L_b. In the view of the discussion of section 5.2, this would be the case of patches of at most a kilometric size, but probably much smaller. Such small patches would certainly escape from detection and they could in no way correspond to the superficial creep reported in the literature, which involves decakilometric to hectokilometric regions. We conclude that the velocity-weakening scenario is very unlikely, and are in favor of superficial afterslip related to permanent velocity strengthening regions.

5.5. On Fault Rheology

[70] The transients described here are not possible under a pure velocity strengthening rheology, or assuming that the frictional stress is always steady state, as it would be if $d_c = 0$. Therefore a key ingredient is the existence of a finite amount of slip d_c needed to evolve from one steady state to the other. Acceleration transients are essentially due to the unstable feedback between two ingredients: a viscous component and a slip-weakening component. We do not expect the particular mathematical form of the fault zone constitutive law to be essential for the phenomenology described here, as long as these two ingredients are present. In rate-and-state friction these correspond respectively to the direct effect and to the dominantly slip-weakening character of the evolution effect far above steady state [*Beeler*, 2004]. However, any power law creep rheology appended by an evolution effect would result in qualitatively similar results. Given current uncertainties about the proper rheology of the deep crust it is better to keep an open mind in model-dependent interpretations of observations.

[71] In this article, we have systematically compared the predictions of two usual laws for the evolution of the state variable, the aging law and the slip law (equations (6) and (7), respectively). Overall, the responses are qualitatively similar, but some quantitative differences exist. In the case of perturbations increasing the Coulomb stress, we found that the slip law predicts a stronger response than the aging law. The converse is true in the case of negative perturbations in the Coulomb stress. The slip and aging law have

were originally motivated by laboratory experiments with small to moderate velocity steps. Recently, *Bayart et al.* [2006] performed finite velocity steps (up to 100 times the loading velocity) and found that only the slip law could properly model their data. Such large velocity steps correspond to $\Omega \gg 1$ as expected near the rupture front. It should be kept in mind that the results of *Bayart et al.* [2006] were obtained at room temperature. Velocity step experiments in the velocity strengthening regime close to the transition zone ($a \gtrsim b$), in the temperature range 250–300°C for granite, should allow the discrimination of the evolution laws. The analytical results presented here should be particularly helpful to analyze those laboratory results.

6. Conclusion

[72] We have studied the dynamics of a rate-and-state strengthening fault in response to localized static stress perturbations. Positive Coulomb stress changes induce slip acceleration followed by relaxation toward steady state. Our simulations and theoretical arguments show that the evolution of slip during such transients is strikingly similar to the earthquake nucleation process on a weakening fault, with an initial phase of slip localization and acceleration, followed by the propagation of a quasi-static crack. On strengthening faults; however, slip rate eventually relaxes back to steady state.

[73] In fault zones close to velocity neutral ($a \approx b$), as expected right below the seismogenic zone, the peak sliding velocity can be extremely large and reach dynamic scales. Large-amplitude transients could propagate updip and trigger a seismic event in the seismogenic region above, especially near the end of the seismic cycle, as proposed by *Rogers and Dragert* [2003]. The time to peak velocity decreases with increasing amplitude and wavelength of the positive stress perturbation, consistently with the behavior of a spring block model.

[74] The short duration of the slip acceleration transient justifies the usual practice of modeling postseismic slip under the steady state approximation, which reduces the rate-and-state rheology to a pure velocity-strengthening rheology. This approach yields a constraint on the frictional parameter $a - b$, but the apparent initial velocity should be interpreted as the peak velocity of the short initial transient. Conversely, modeling postseismic geodetic data with the complete rate-and-state rheology is justified if the initial acceleration transient is observable. In this approach, proper resolution requires, even on strengthening regions, grid sizes smaller than $L_b = G\, d_c/b\sigma$ with the aging law and up to 20 times smaller with the slip law. This is more stringent than the resolution criterion based on the critical length $L_c = Gd_c/(b - a)\sigma$ [*Rice*, 1993] commonly adopted in the literature [e.g., *Hirose and Hirahara*, 2004; *Liu and Rice*, 2005]. In full rate-and-state inversions, current limitations on computational resources will tend to bias the parameter space to high values of $d_c/b\sigma$.

[75] Our results suggest that shallow afterslip observed at expectedly seismogenic depths occurs on intrinsically creeping zones, with rate-and-state strengthening rheology. This is consistent with the observed location of postseismic slip of the 2005 M_w 8.7 Nias earthquake [*Hsu et al.*, 2006], in areas that were also creeping during the interseismic period [*Chlieh et al.*, 2008].

[76] Creep transients can be also triggered by negative Coulomb stress changes, representing for example a sudden increase in effective normal stress induced by the rupture of a high pressure fluid pocket. Their peak slip velocity is attained at much longer timescales and remains limited to a few orders of magnitude larger than the plate velocity. Because they occur long after their cause, these transients may be misinterpreted as spontaneous slow earthquakes. Some slow events exhibiting a rather modest peak velocity may be triggered by sudden episodes of fluid release.

Appendix A: Condition for Well Resolved Spatial Discretization

[77] The presence of a characteristic slip scale d_c in the aging state evolution law (equation (6)) implies a finite effective slip-weakening rate $b\sigma/d_c$ for sliding far above steady state, which in turn implies the existence of a characteristic length scale L_b (equation (10)). The smallest scale of slip localization is $L_v = 1.3774\ L_b$ [*Rubin and Ampuero*, 2005] and the size of the crack tip process zone is $\approx 0.7 L_b$ [*Ampuero and Rubin*, 2008, Figure 10]. Obviously, these length scales must be well resolved by the spatial discretization of the governing elasticity and rate-and-state equations ($\Delta x \ll L_b$) in order to obtain an accurate numerical solution. A more subtle issue, illustrated in the remainder of this appendix, is that the risk of numerical instabilities is high if the condition $\Delta x \ll L_b$ is not verified, even on a strengthening fault. In all our simulations with the aging law we have set $\Delta x \leq L_b/20$.

[78] Figure A1 shows the evolution of the maximum velocity on a rate-and-state strengthening fault segment of size $L = 300\ L_b$, with $b/a = 0.9$ and governed by the aging law, following a perturbation of size $R_0 = 150\ L_b$ and amplitude $\Delta\tau_0 = 10\ a\sigma$. The different curves result from the numerical solution of the 2-D model with different grid sizes, $\Delta x/L_b = 1/16$, 1/4, 4, and 16. The heavy grey line is the solution for $\Delta x/L_b = 1/16$ and further reduction of Δx does not yield visible changes. Looking at the inset of Figure A1 near the peak velocity of the well resolved case (thick line), periodic fluctuations of the sliding velocity around the maximum value are observed when the numerical grid is too coarse. The amplitude and period of those oscillations increase with the size of the grid. These are numerical artifacts that are not present on a sufficiently refined grid. Figure A2 shows the result of a similar exercise now with $\Delta\tau_0 = -10a\sigma$. In this case, a coarse mesh yields secondary maxima in slip velocity in some cases one order of magnitude larger than the well resolved case. As in the case $\Delta\tau_0 = +10a\sigma$, the period and amplitude of the secondary velocity peaks are increasing with the size of the grid and disappear for a sufficiently refined grid. Consequently, the effect of a rough discretization is worse in the case of negative steps in Coulomb stress that it is in the case of positive steps in Coulomb stress.

[79] The properties of the secondary peaks in Figure A2 can be understood by the following reasoning. When $\Delta x > L_b$ each cell can slip independently from its neighbors. As the slip front is propagating towards the center of the fault, it triggers the acceleration of each individual point it

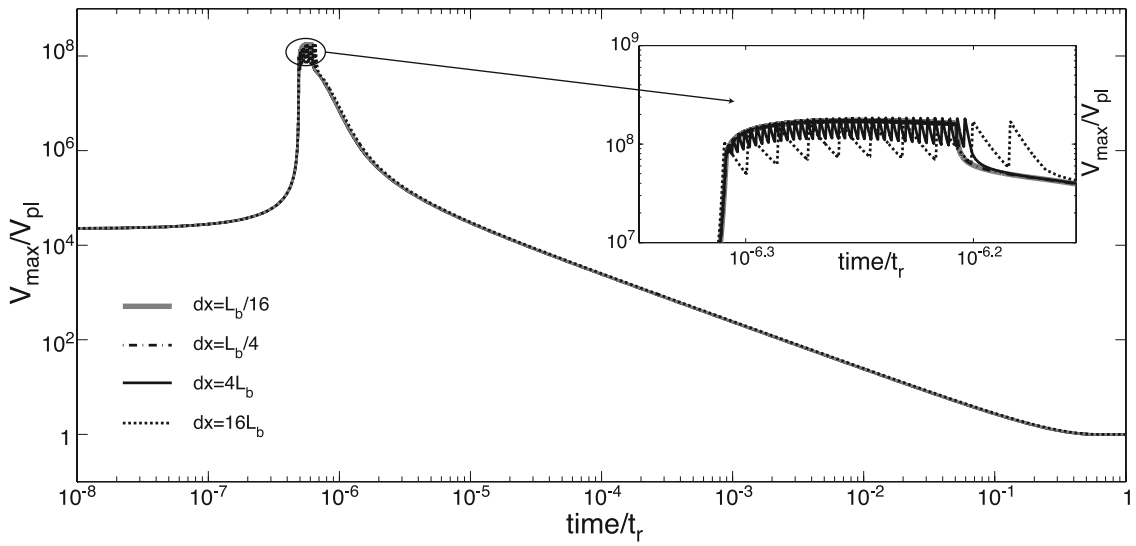

Figure A1. Response of a 2-D creeping fault of size $L = 300\ L_b$, with $b/a = 0.9$ and governed by the aging law, following a perturbation of size $R_0 = 150\ L_b$ and amplitude $\Delta\tau_0 = 10a\sigma$. Various grid size are considered ($\Delta x/L_b = 1/16$, 1/4, 4, and 16). The stable solution (thick solid grey line) is achieved when the grid size becomes significantly smaller than L_b.

encounters. Therefore, the period of those secondary peaks corresponds roughly to $\Delta x/V_{prop}$, the time needed for the front to propagate from one point to its immediate neighbor, an estimate of V_{prop} being given in equation (33). As predicted by a 1-D model, the larger the ratio $\Delta x/L_b$, the higher the velocity of a secondary peak.

[80] For the slip law, equation (7), the grid resolution requirements are more stringent. The localization length and the size of the process zone are smaller than L_b by a factor that depends logarithmically on slip rate, and that typically reaches ≈20 during fast slip [*Ampuero and Rubin*, 2008]. Moreover, the slip law is more unstable to finite amplitude perturbations than the aging law. In all our simulations with the slip law we have set $\Delta x < L_b/200$.

[81] According to the criterion introduced by *Rice* [1993], when Δx is larger than the critical length L_c of equation (19) the continuity of the medium is lost and the numerical calculation becomes "inherently discrete": a numerical cell can generate an instability independently of the neighboring cells. A stability criteria based on L_c fails to explain our results of Figures A1 and A2, because L_c is undefined (negative) on a velocity strengthening region. The critical length L_c obtained from a linear stability analysis is not relevant for the perturbations of finite amplitude considered

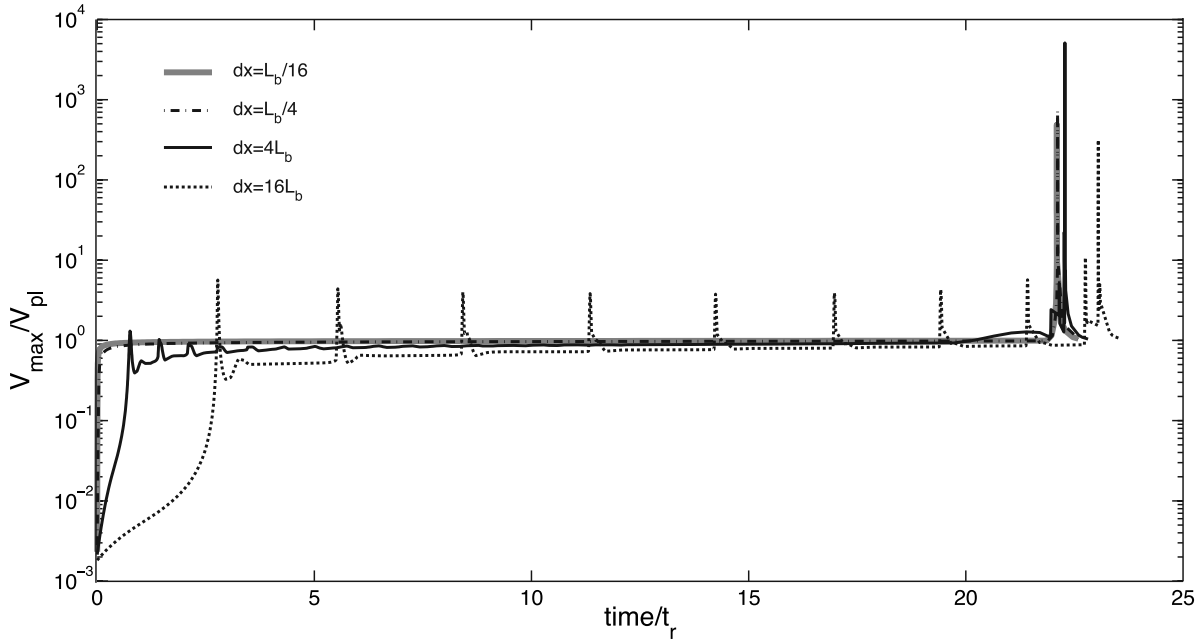

Figure A2. Same as Figure A1 for an unloading stress change $\Delta\tau_0 = -10a\sigma$.

here. The same conclusions have been reached by *Dieterich* [1992] and *Rubin and Ampuero* [2005] considering rate-and-state weakening faults.

[82] Examples of low resolution (low $L_b/\Delta x$) in rate-and-state simulations are unfortunately abundant, due to the widespread adoption of a criterion based on L_c [*Rice*, 1993]. Values of $L_b/\Delta x$ at seismogenic depths and in part of the transition zones are typically of order 1 in many recent simulations exploring specifically slow slip phenomena [*Liu and Rice*, 2005; *Hirose and Hirahara*, 2004; *Shibazaki and Shimamoto*, 2007].

[83] The stability problems may not affect the timing of the episode of slip increase (regular earthquakes or creep bursts) as illustrated in Figure A1. Nevertheless, a careful look at the numerical data reveals the existence of secondary oscillations, which period and amplitude increase as $\Delta x/L_b$ decrease. A lack of resolution can lead to dramatic numerical artifacts as illustrated by Figure A2, that may be misinterpreted as physically sound slip instabilities.

Appendix B: Slip Instabilities in a 1-D Model

B1. Self-Accelerating Instabilities on a Weakening Spring Block

[84] We consider a single spring block system without inertia nor radiation damping. This 1-D model temptatively represents a spatial average of a higher dimensional fault model, with effective stiffness K scaled as

$$K = \gamma \frac{G}{L}, \tag{B1}$$

where L is a typical shortest dimension of the slipping region and γ is a factor of the order of unity that depends on the patch shape, on the sliding mode and on Poisson's ratio. For the purpose of comparison with multidimensional models we set $\gamma = \pi$. However, the analogy must be exercised with caution when the dimensions of the slipping patch are evolving with time.

[85] During fast sliding rate-and-state faults evolve often far above steady state, $\Omega = V\theta/d_c \gg 1$. This is typically the case when a fault initially sliding at steady state velocity V_{pl} is perturbed by a large increase of shear stress $\Delta\tau_0 \gg a\sigma$ since, from equation (3),

$$\Omega^+ = V^+/V_{pl} = \exp(\Delta\tau_0/a\sigma). \tag{B2}$$

If the state variable is governed by the aging law, the condition $\Omega \gg 1$ allows for the so-called self-accelerating approximation, in which equation (6) becomes $\dot{\theta} \approx -\Omega$. In this regime [*Dieterich*, 1994] obtained the following solution for slip velocity

$$V(t) = \frac{V^+}{(1+\Lambda)\, e^{-t/t_r} - \Lambda}\ , \tag{B3}$$

where the initial velocity V^+ is given by equation (3),

$$\Lambda = \frac{K_b - K}{K} \frac{V^+}{V_{pl}}, \tag{B4}$$

the characteristic stiffness K_b is given in equation (13) and the characteristic time t_r is defined as

$$t_r = \frac{a\sigma}{K V_{pl}}. \tag{B5}$$

If $K < K_b$ slip accelerates and becomes unbounded at failure time

$$t^* = t_r \ln(1 + 1/\Lambda). \tag{B6}$$

It can be shown, following the formalism developed by *Perfettini et al.* [2003], that equation (B6) gives a lower bound of the time to instability when the self-accelerating approximation is relaxed. The approximation relies on the assumption that $\Omega \gg 1$ persists until failure, and we verify next its self-consistency by seeking an expression for $\Omega(t)$.

[86] The equation of equilibrium for the spring block model, a balance between frictional and elastic forces, is

$$\sigma\mu(V,\theta) = K\big(V_{pl}\ t - D\big), \tag{B7}$$

where σ is the normal stress (assumed constant), the friction coefficient μ is given by the rate-and-state law (5), V_{pl} is the long-term loading velocity and D is slip. Deriving with respect to time the equilibrium equation (B7) and the definition $\Omega = V\theta/d_c$, we obtain

$$a\sigma\frac{\dot{V}}{V} + b\sigma\frac{\dot{\theta}}{\theta} = K\big(V_{pl} - V\big) \tag{B8}$$

$$\frac{\dot{\Omega}}{\Omega} = \frac{\dot{V}}{V} + \frac{\dot{\theta}}{\theta} \tag{B9}$$

respectively. When $\Omega \gg 1$, we can insert $\dot{\theta}/\theta \approx -V/d_c$ in the equations above and, after some algebra,

$$\frac{\dot{\Omega}}{\Omega} = \frac{K_c - K}{K_b - K}\frac{\dot{V}}{V} + \frac{K}{K_b - K}\frac{V_{pl}}{d_c} \tag{B10}$$

where

$$K_c = \frac{(b-a)\sigma}{d_c} \tag{B11}$$

Upon time integration and considering equation (B5), we obtain

$$\frac{\Omega(t)}{\Omega^+} = \left(\frac{V(t)}{V^+}\right)^{\frac{K_c-K}{K_b-K}} \exp\left(\frac{K_b - K_c}{K_b - K}\frac{t}{t_r}\right) \tag{B12}$$

or, eliminating t in favor of $V(t)$ with the aid of equation (B3),

$$\frac{\Omega(t)}{\Omega^+} = \left(\frac{V(t)}{V^+}\right)^{\frac{K_c-K}{K_b-K}} \left(\frac{1+\Lambda}{V^+/V(t) + \Lambda}\right)^{\frac{K_b-K_c}{K_b-K}} \tag{B13}$$

Whereas equation (B3) shows that slip initially accelerates toward failure if $K < K_b$, it appears from equation (B13) that the fault is guaranteed to remain above steady state (increasing Ω) up to failure time only if $K < K_c$. If

$K_c < K < K_b$ the evolution of Ω is eventually dominated by the decay of the first term of equation (B13) and the instability is frustrated, although it can reach high velocities if the initial perturbation is strong enough. If $K > K_b$ no instability develops: according to equation (B3), V relaxes toward $-V^+/\Lambda$ and the second term in equation (B13) decays, bringing the fault back to steady state.

[87] The critical stiffness K_c for self-accelerating instabilities appears also in classical linear stability analysis, but it is obtained here from a more general, nonlinear analysis consistent with the results of *Ranjith and Rice* [1999]. *Rubin and Ampuero* [2005] and *Ampuero and Rubin* [2008] presented a similar discussion but assuming slow loading ($V_{pl} \ll V$ in equation (B8), which implies the second term in equation (B13) is neglected).

B2. Response of a Strengthening Spring Block to Positive Stress Perturbations

[88] The sign of $a - b$ is not involved in equation (B3) so, although originally derived for weakening faults, this self-accelerating regime also exists for strengthening faults if the initial conditions are such that $\Omega \gg 1$. The main difference on a strengthening fault is that, as $K_c < 0$, it is always the case that $K > K_c$ and instabilities do not fully develop. However, although $V(t)$ remains finite its transient excursions can be large. We focus next on the extremal properties of these transients, their peak velocity $V_{\max}$ and the time $t_{\max}$ needed to attain peak velocity.

[89] When $K > K_b$ the slip velocity decays monotonically if $(K - K_b)V^+/KV_{pl} > 1$ and the peak velocity $V_{\max} = V^+$ is reached at $t_{\max} = 0$. When $K < K_b$ transients with initial acceleration occur and $V_{\max}$ is reached close to the time when steady state is recovered. At the expense of a slight overestimation of $V_{\max}$ and underestimation of $t_{\max}$, equation (B13) obtained under the assumption $\Omega \gg 1$ can be combined with the condition $\Omega \approx 1$ to yield an implicit relation for $V_{\max}$:

$$\frac{V_{\max}}{V_{pl}} = \left(\frac{V^+}{V_{pl}} \frac{1+\Lambda}{V^+/V_{\max} + \Lambda} \right)^{\frac{K_b - K_c}{K - K_c}}. \tag{B14}$$

A close form expression,

$$\frac{V_{\max}}{V_{pl}} = \left(\frac{V^+}{V_{pl}} (1 + 1/\Lambda) \right)^{\frac{K_b - K_c}{K - K_c}}, \tag{B15}$$

is obtained when $V_{\max} \gg V^+/\Lambda = V_{pl} \times K/(K_b - K)$, which can be shown to be generally valid if K and V^+ are not too close to K_b and V_{pl}, respectively. Moreover, under these conditions, the time of peak velocity, $t_{\max}$, is given by the time to instability t^* of equation (B6).

[90] Further simplifications can be obtained in the limit $K \ll K_b$:

$$\frac{V_{\max}}{V_{pl}} \approx \left(\frac{V^+}{V_{pl}} \right)^{\frac{a}{a-b}} = \exp\left(\frac{\Delta\tau}{(a-b)\sigma} \right), \tag{B16}$$

$$t_{\max} \approx \frac{a}{b} \frac{d_c}{V^+} = t_r \frac{K}{K_b} \exp\left(-\frac{\Delta\tau}{a\sigma} \right) \tag{B17}$$

Close to velocity neutral ($a \approx b$), the maximum velocity can be much larger than the loading velocity V_{pl}, and reached on a timescale much shorter than t_r.

[91] We now focus on the relaxation phase. Close to $t_{\max}$, $\dot{V} \approx 0$, $\Omega \approx 1$ and, for a strong transient, $V \gg V_{pl}$, thus equation (B8) yields

$$\dot{\theta}(t_{\max}) \approx -\frac{K}{K_b} \tag{B18}$$

Using $\ddot{\theta} = -\dot{\Omega}$ together with equation (B9) gives $\ddot{\theta} = -\Omega(\frac{\dot{\theta}}{\theta} + \frac{\dot{V}}{V})$, which simplifies into

$$\ddot{\theta}(t_{\max}) \approx \frac{K}{K_b} \frac{1}{\theta(t_{\max})} = \frac{V_{\max}}{d_c} \frac{K}{K_b}, \tag{B19}$$

after use of equation (B18), $\Omega(t_{\max}) \approx 1$, and $\theta(t_{\max}) \approx \frac{d_c}{V_{\max}}$. In the limit $K \ll K_b$ equations (B18) and (B19) predict that $\dot{\theta}(t_{\max}) \to 0$ and $\ddot{\theta}(t_{\max}) \to 0$. Consequently, a very compliant system relaxes in steady state once it has reached its peak velocity and its frictional stress decays with velocity according to (8) for $t > t_{\max}$. This behavior is analogous to the relaxation of a pure rate-strengthening fault ($a > 0$, $b = 0$) for which the parameter a would be replaced by $a - b$. Following *Perfettini et al.* [2005], from time $t_{\max}$ the velocity decreases as

$$V(t') = \frac{V_{\max}\, e^{t'/t_r'}}{1 + \frac{V_{\max}}{V_{pl}} \left(e^{t'/t_r'} - 1 \right)}, \tag{B20}$$

where $V_{\max}$ is given by (B15), $t' = t - t_{\max}$, and

$$t_r' = \frac{(a-b)\sigma}{KV_{pl}}. \tag{B21}$$

Typically, $t_{\max} \ll t_r'$, so $t' \approx t$. We emphasize, however, that if the condition $K \ll K_b$ is not fulfilled then the relaxation phase starts with an incursion above steady state.

B3. Response of a Strengthening Spring-Block to Negative Stress Perturbations

[92] Immediately after a large unloading shear stress step, $\Delta\tau \ll -a\sigma$, on a fault initially sliding at the steady state velocity V_{pl}, fault slip slows down dramatically, $V^+/V_{pl} \ll 1$ (from equation (3)). To a good approximation during most of the subsequent motion $\theta \approx 1$ (implying $\theta(t) \approx d_c/V_{pl} + t$) and the fault is practically at rest ($V \ll V_{pl}$, except near instability). These approximations also hold on a rate-and-state weakening fault that has just ruptured, and remains valid during most of the interseismic period until it is violated at the end of the earthquake cycle, when nucleation is underway.

[93] Equation (B8) reduces to

$$\frac{\dot{V}}{V} \approx \frac{1}{t_r} \left(1 - \frac{K_b/K}{1 + \frac{V_{pl}t}{d_c}} \right). \tag{B22}$$

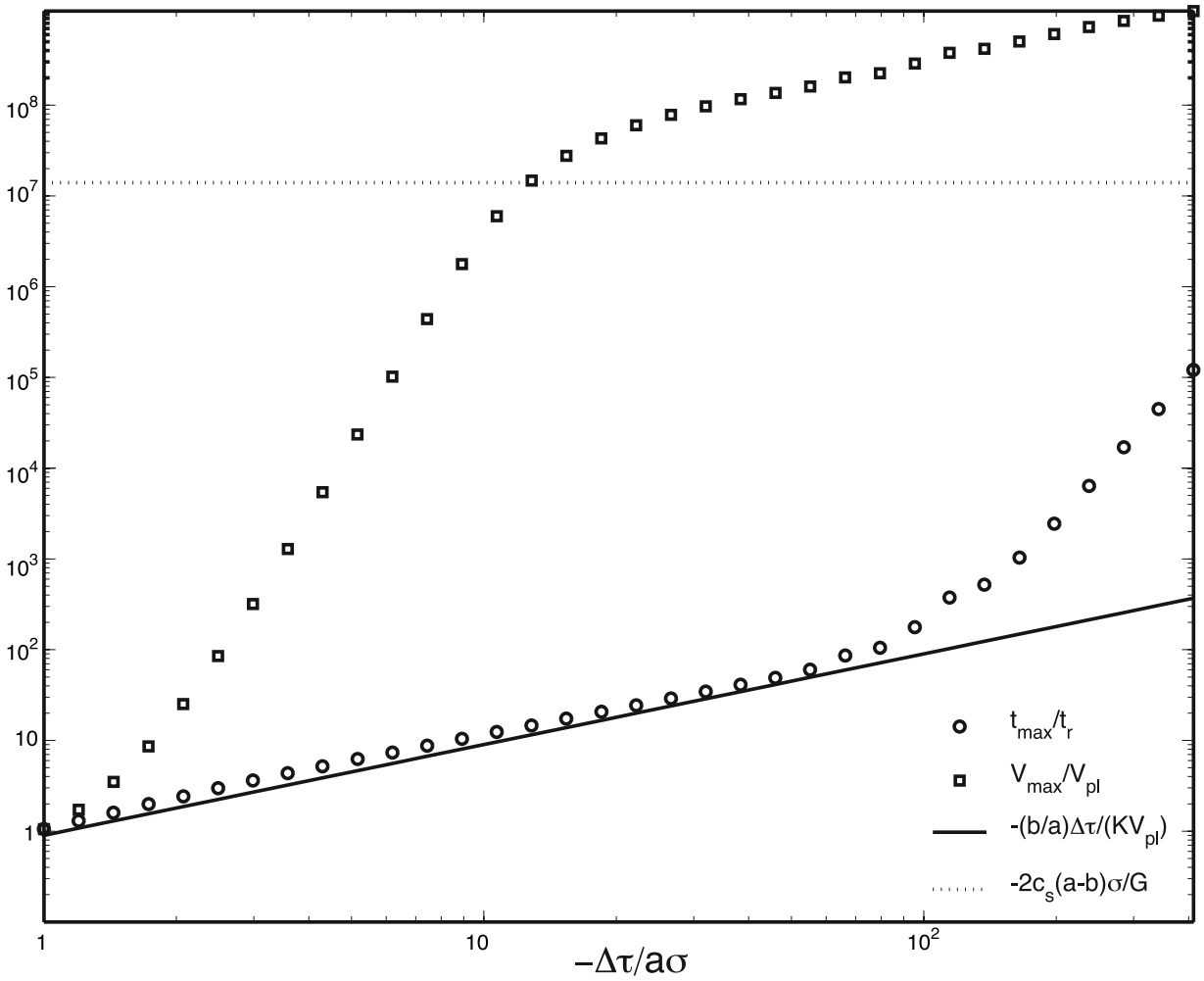

Figure B1. Time to instability and maximum velocity as a function of the amplitude of the perturbation $\Delta\tau < 0$ considering a 1-D model. The horizontal dashed line corresponds to the velocity $V_{dyn}{}' = \frac{2c_s(a-b)\sigma}{G}$ above which dynamic effects are significant. The continuous line is the prediction of equation (B26) for the time to instability.

This predicts initial deceleration if $K < K_b$, followed by acceleration towards instability after time

$$t_1 = (K_b/K - 1)\frac{d_c}{V_{pl}} \tag{B23}$$

[94] Equations (B8) and (B9) with $V \ll V_{pl}$ give

$$\frac{\dot{\Omega}}{\Omega} = \frac{b-a}{b}\frac{\dot{V}}{V} + \frac{K}{b\sigma}V_{pl}. \tag{B24}$$

Integrating with respect to time,

$$\frac{\Omega(t)}{\Omega^+} \approx \left(\frac{V(t)}{V^+}\right)^{\frac{b-a}{b}} \exp\left(\frac{a}{b}\frac{t}{t_r}\right), \tag{B25}$$

The second term on the right side of equation (B25) is always positive so that it contributes to increase Ω and to drive the fault toward instability. The first term increases with V when $b > a$, so that on a weakening fault Ω will not cease to increase, ultimately leading to instability. On a strengthening fault ($a > b$) this term tends to decrease Ω when V increases, so it has instead a stabilizing effect. The considerations following equation (B24) are valid for both the aging and the slip law.

[95] The time of peak transient velocity $t_{\max}$ is of the same order as the time to reach again steady state. For large decreases in shear stress ($\Omega_+ = V^+/V_{pl} \ll 1$) the exponential term in equation (B25) dominates and a rough estimate, setting $\Omega(t_{\max}) \approx 1$ and considering also equation (B2), is

$$t_{\max} \approx -\frac{b}{a}\frac{\Delta\tau_0}{KV_{pl}}, \tag{B26}$$

If $a = b$, equation (B26) agrees with the prediction of a Coulomb failure model, for which failure occurs at a fixed stress threshold: it is the time needed for the tectonic load to reload a fault at rest by an amount equal to the stress drop $\Delta\tau_0$.

[96] Figure B1 shows numerical simulation results on a spring block model with radiation damping in response to a perturbation of amplitude $\Delta\tau < -a\sigma$ (weaker perturbations

lead to very low $V_{\max} \approx V_{pl}$). The maximum velocity $V_{\max}$ grows with $|\Delta\tau|$, in contrast with the behavior on multidimensional fault models described in section 4.2. Two regimes are separated by the velocity scale

$$V'_{dyn} = \frac{2c_s(a-b)\sigma}{G}, \tag{B27}$$

at which the dynamic effect of radiation damping becomes significant [*Rubin and Ampuero*, 2005]. The time to instability $t_{\max}$ also grows with $|\Delta\tau|$ and, for low $|\Delta\tau|$, it is well described by equation (B26).

Notation

Variable	Definition
a	first constitutive parameter
b	second constitutive parameter
$a' = a - b$	constitutive parameter for the pure velocity strengthening rheology
d_c	characteristic distance for the state evolution
G	shear modulus
μ	friction coefficient
V_*	reference velocity
μ_*	reference friction coefficient
v	Poisson's ratio
c_s	shear wave velocity
V_{pl}	plate velocity
$\Delta\tau_0$	amplitude of the static stress step
R_0	radius of the static stress step
L	characteristic size of the creeping patch
$\dot{\epsilon}$	strain rate
D	slip
V	slip velocity
V^+	sliding velocity immediately after the onset of the stress perturbation
$V_{dyn} = \frac{2a\sigma c_s}{G}$	velocity scale for the onset of dynamic effects
θ	state variable
θ_i	value of the state variable before the arrival of the rupture front
τ	frictional stress
σ	normal stress
τ_0	stress due to external load
$\Omega = \frac{V\theta}{d_c}$	distance to steady state
t	time
t_*	time to reach infinite velocity
$V_{\max}$	maximal velocity
V_{prop}	propagation velocity
$t_{\max}$	time to reach $V_{\max}$
t_1	duration of the deceleration phase for unloading steps
$t_r = \frac{a\sigma}{KV_{pl}}$	characteristic relaxation time
L_b	localization (or nucleation) length for the aging law
L_b'	localization (or nucleation) length for the slip law
L_v	minimal localization length
L_∞	maximal size in the crack-like expansion phase
$K_c = \frac{(b-a)\sigma}{d_c}$	critical stiffness
$K_b = \frac{b\sigma}{d_c}$	stiffness associated with L_b
$K_v = 0.6219\ K_b$	stiffness associated with L_v
Δx	numerical grid size

[97] **Acknowledgments.** We thank the associate editor and an anonymous reviewer for useful comments. This paper benefited from fruitful discussions with Allan Rubin, Jean-Philippe Avouac, and Alon Ziv.

References

Ampuero, J. P., and A. M. Rubin (2008), Earthquake nucleation on rate and state faults: Aging and slip laws, *J. Geophys. Res.*, *113*, B01302, doi:10.1029/2007JB005082.

Bayart, E., A. M. Rubin, and C. Marone (2006), Evolution of fault friction following large velocity jumps, *Eos Trans. AGU*, *87*(52), Fall Meet. Suppl., Abstract S31A–0180.

Beeler, N. M. (2004), Review of the physical basis of laboratory-derived relations for brittle failure and their implications for earthquake occurrence and earthquake nucleation, *Pure Appl. Geophys.*, *161*, 1853–1876.

Blanpied, M. L., D. A. Lockner, and J. D. Byerlee (1995), Frictional slip of granite at hydrothermal conditions, *J. Geophys. Res.*, *100*, 13,045–13,064.

Burgmann, R., S. Ergintav, P. Segall, E. Hearn, S. McClusky, R. Reilinger, H. Woith, and J. Zschau (2002), Time-space variable afterslip on and deep below the Izmit earthquake rupture, *Bull. Seismol. Soc. Am.*, *92*, 126–137.

Chang, C., Y. Wu, L. Zhao, and F. Wu (2007), Aftershocks of the 1999 Chi-Chi Taiwan Earthquake: The first hour, *Bull. Seismol. Soc. Am.*, *96*, 807–820.

Chlieh, M., J. de Chabalier, J. Ruegg, R. Armijo, R. Dmowska, J. Campos, and K. Feigl (2004), Crustal deformation and fault slip during the seismic slip in the North Chile subduction zone, from GPS and InSAR observations, *Geophys. J. Int.*, *157*, 1–17.

Chlieh, M., et al. (2007), Coseismic slip and afterslip of the Great (M_w 9.15) Sumatra-Andaman earthquake of 2004, *Bull. Seismol. Soc. Am.*, *97*, 152–173, doi:10.1785/0120050631.

Chlieh, M., J.-P. Avouac, K. Sieh, D. Natawidjaja, and J. Galetzka (2008), Heterogeneous coupling on the Sumatran megathrust constrained from geodetic and paleogeodetic measurements, *J. Geophys. Res.*, *113*, B05305, doi:10.1029/2007JB004981.

Chouet, B. (1992), A seismic model for the source of long-period events and harmonic tremor, in *Volcanic Seismology*, edited by P. Gasparini, R. Scarpa, and K. Aki, pp. 133–156. Springer, Berlin.

Cochard, A., and J. R. Rice (1997), A spectral method for numerical elastodynamic fracture analysis without spatial replication of the rupture event, *J. Mech. Phys. Solids*, *45*, 1393–1418.

Crescentini, L., A. Amoruso, and R. Scarpa (1999), Constraints on slow earthquake dynamics from a swarm in central Italy, *Science*, *286*, 2132–2134.

Dieterich, J. H. (1979), Modeling of rock friction: 1. Experimental results and constitutive equations, *J. Geophys. Res.*, *84*, 2161–2168.

Dieterich, J. H. (1981), Constitutive properties of faults with simulated gouge, in *Mechanical Behavior of Crustal Rocks*, *Geophys. Monogr. Ser.*, vol. 24, edited by N. L. Carter et al., pp. 103–120. AGU, Washington, D.C.

Dieterich, J. H. (1992), Earthquake nucleation on faults with rate- and state-dependent strength, *Tectonophysics*, *211*, 115–134.

Dieterich, J. H. (1994), A constitutive law for rate of earthquake production and its application to earthquake clustering, *J. Geophys. Res.*, *99*, 2601–2618.

Douglas, A., J. Beavan, L. Wallace, and J. Townend (2005), Slow slip on the northern Hikurangi subduction interface, New Zealand, *Geophys. Res. Lett.*, *32*, L16305, doi:10.1029/2005GL023607.

Dragert, H. (2007), Mediating plate convergence, *Science*, *315*, 471–472.

Dragert, H., K. Wang, and T. James (2001), A silent slip event on the deeper Cascadia subduction interface, *Science*, *292*, 1525–1528.

Ferrazzini, V., and K. Aki (1992), Preliminary results from a field experiment on volcanic events at Kilauea using an array of digital seismographs, in *Volcanic Seismology*, edited by P. Gasparini, R. Scarpa, and K. Aki, pp. 168–189. Springer, Berlin.

Fialko, Y. (2004), Evidence of fluid-filled upper crust from observations of postseismic deformation due to the 1992 M_w7.3 Landers earthquake, *J. Geophys. Res.*, *109*, B08401, doi:10.1029/2004JB002985.

Gu, J., J. R. Rice, A. L. Ruina, and S. T. Tse (1984), Slip motion and stability of a single degree of freedom elastic system with rate and state dependent friction, *J. Mech. Phys. Solids*, *32*, 167–196.

Hearn, E., R. Burgmann, and R. Reilinger (2002), Dynamics of Izmit earthquake postseismic deformation and loading of the Duzce earthquake hypocenter, *Bull. Seismol. Soc. Am.*, *92*, 172–193.

Hillers, G., P. M. Mai, Y. Ben-Zion, and J. P. Ampuero (2007), Statistical properties of seismicity of fault zones at different evolutionary stages, *Geophys. J. Int.*, *169*, 515–533.

Hirose, H., and K. Hirahara (2004), A 3-D quasi-static model for a variety of slip behaviors on a subduction fault, *Pure Appl. Geophys.*, *161*, 2417–2431.

Hirose, H., K. Hirahara, F. Kimata, N. Fujii, and S. Miyazaki (1999), A slow thrust slip event following the two 1996 Hyuganada earthquakes beneath the Bungo Channel, southwest Japan, *Geophys. Res. Lett.*, *21*, 3237–3240.

Hsu, Y.-J., N. Bechor, P. Segall, S.-B. Yu, L.-C. Kuo, and K.-F. Ma (2002), Rapid afterslip following the 1999 Chi-Chi, Taiwan earthquake, *Geophys. Res. Lett.*, *29*(16), 1754, doi:10.1029/2002GL014967.

Hsu, Y.-J., M. Simons, J.-P. Avouac, J. Galtezka, K. Sieh, M. Chlieh, D. Natawidjaja, L. Prawirodirdjo, and Y. Bock (2006), Frictional afterslip following the 2005 Nias-Simeulue Earthquake, Sumatra, *Science*, *312*, 1921–1926.

Ito, Y., K. Obara, K. Shiomi, S. Sekine, and H. Hirose (2007), Slow earthquakes coincident with episodic tremors and slow slip events, *Science*, *315*, 503–506.

Kao, H., S.-J. Shan, H. Dragert, G. Rogers, J. Cassidy, and K. Ramachandran (2005), A wide depth distribution of seismic tremors along the northern Cascadia margin, *Nature*, *436*, 841–844, doi:10.1038/nature03903.

Katsumata, K., M. Kasahara, S. Ozawa, and A. Ivashchenko (2002), A five years super-slow precursor model for the 1984 M8.3 Hokkaido-Toho-Oko lithospheric earthquake based on tide gauge data, *Geophys. Res. Lett.*, *29*(13), 1654, doi:10.1029/2002GL014982.

Langbein, J., J. Murray, and H. Snyder (2006), Coseismic and initial postseismic deformation from the 2004 Parkfield, California, earthquake, observed by global positioning system, electronic distance meter, creepmeters, and borehole strainmeters, *Bull. Seismol. Soc. Am.*, *96*, 5304–5320.

Linde, A., M. Gladwin, M. Johnson, R. Gwyther, and R. Bilham (1996), A slow earthquake sequence on the San Andreas fault, *Nature*, *383*, 65–68.

Liu, Y., and J. Rice (2005), Aseismic slip transients emerge spontaneously in three-dimensional rate and state modeling of subduction earthquake sequences, *J. Geophys. Res.*, *110*, B08307, doi:10.1029/2004JB003424.

Lowry, A., K. Larson, V. Kostoglodov, and R. Bilham (2001), Transient fault slip in Guerrero, southern Mexico, *Geophys. Res. Lett.*, *28*, 3753–3756.

Marone, C. (1998), Laboratory-derived friction laws and their application to seismic faulting, *Annu. Rev. Eath Planet. Sci.*, *26*, 643–696.

Marone, C., and B. Kilgore (1993), Scaling of the critical slip distance for seismic faulting with shear strain in fault zones, *Nature*, *362*, 618–621.

Marone, C. J., C. H. Scholz, and R. Bilham (1991), On the mechanics of earthquake afterslip, *J. Geophys. Res.*, *96*, 8441–8452.

Melbourne, T., and F. Webb (2002), Precursory transient slip during the 2001 M_w = 8.4 Peru earthquake sequence from continuous GPS, *Geophys. Res. Lett.*, *29*(21), 2032, doi:10.1029/2002GL015533.

Miller, M., T. Melbourne, D. Johnson, and W. Sumner (2002), Periodic slow earthquakes from the Cascadia subduction zone, *Science*, *295*, 2344–2345.

Miyazaki, S., P. Segall, J. Fukuda, and T. Kato (2004), Space time distribution afterslip following the 2003 Tokachi-Oki earthquake: Implications for variations in fault zone frictional properties, *Geophys. Res. Lett.*, *31*, L06623, doi:10.1029/2003GL019410.

Miyazaki, S., P. Segall, J. McGuire, T. Kato, and Y. Hatanaka (2006), Spatial and temporal evolution of stress and slip rate during the 2000 Tokai slow earthquake, *J. Geophys. Res.*, *111*, B03409, doi:10.1029/2004JB003426.

Nadeau, R. M., and D. Dolenc (2005), Nonvolcanic tremors deep beneath the San Andreas fault, *Science*, *307*, 389–507.

Nakatani, M. (2001), Conceptual and physical clarification of rate and state friction: Frictional sliding as thermally activated rheology, *J. Geophys. Res.*, *106*, 13,347–13,380.

Obara, K. (2002), Nonvolcanic deep tremor associated with subduction in southwest Japan, *Science*, *296*, 1679–1681.

Obara, K., H. Hirose, F. Yamamizu, and K. Kasahara (2004), Episodic slow slip events accompanied by non-volcanic tremors in southwest Japan subduction zone, *Geophys. Res. Lett.*, *31*, L23602, doi:10.1029/2004GL020848.

Okada, Y. (1992), Internal deformation due to shear and tensile faults in a half-space, *Bull. Seismol. Soc. Am.*, *82*, 1018–1040.

Ozawa, S., M. Murakami, and T. Tada (1997), Time-dependent inversion study of the slow thrust event in the Nankai trough subduction zone, southwestern Japan, *Science*, *278*, 834–838.

Perfettini, H., and J.-P. Avouac (2004), Postseismic relaxation driven by brittle creep: A possible mechanism to reconcile geodetic measurements and the decay rate of aftershocks, application to the Chi-Chi earthquake, Taiwan, *J. Geophys. Res.*, *109*, B02304, doi:10.1029/2003JB002488.

Perfettini, H., and J.-P. Avouac (2007), Modelling afterslip and aftershocks following the 1992 Landers Earthquake, *J. Geophys. Res.*, *112*, B07409, doi:10.1029/2006JB004399.

Perfettini, H., J. Schmittbuhl, and A. Cochard (2003), Shear and normal load perturbations on a 2D continuous fault: 1. Static triggering, *J. Geophys. Res.*, *108*(B9), 2408, doi:10.1029/2002JB001804.

Perfettini, H., J.-P. Avouac, and J. Ruegg (2005), Geodetic displacements and aftershocks following the 200 1, M_w = 8.4 Peru earthquake: Implications for the mechanics of the earthquake cycle along subduction zones, *J. Geophys. Res.*, *109*, B09404, doi:10.1029/2004JB003522.

Press, W. H., B. P. Flannery, S. A. Teukolsky, and W. T. Vetterling (1992), Integration of ordinary differential equations, in *Numerical Recipes in C, The Art of Scientific Computing*, 2nd ed., pp. 707–752, Cambridge Univ. Press, Cambridge, U. K.

Pritchard, M., and M. Simons (2006a), An aseismic slip pulse in northern Chile and along-strike variations in seismogenic behavior, *J. Geophys. Res.*, *112*, B08405, doi:10.1029/2006JB004258.

Pritchard, M. E., and M. Simons (2006b), An aseismic slip pulse in northern Chile and along-strike variations in seismogenic behavior, *J. Geophys. Res.*, *111*, B08405, doi:10.1029/2006JB004258.

Ranjith, K., and J. R. Rice (1999), Stability of quasi-static slip in a single degree of freedom elastic system with rate and state dependent friction, *J. Mech. Phys. Solids*, *47*, 1207–1218.

Rice, J. R. (1993), Spatio-temporal complexity of slip on a fault, *J. Geophys. Res.*, *98*, 9885–9907.

Rice, J. R., and A. L. Ruina (1983), Stability of steady frictional slipping, *J. Appl. Mech.*, *50*, 343–349.

Rogers, G., and H. Dragert (2003), Episodic tremor and slip on the Cascadia subduction zone: The chatter of silent slip, *Science*, *300*, 1942–1943.

Rubin, A. M., and J.-P. Ampuero (2005), Earthquake nucleation on (aging) rate and state faults, *J. Geophys. Res.*, *110*, B11312, doi:10.1029/2005JB003686.

Rubinstein, S. M., G. Cohen, and J. Fineberg (2004), Detachment fronts and the onset of dynamic friction, *Nature*, *430*, 1005–1009.

Ruina, A. L. (1983), Slip instability and state variable fricton laws, *J. Geophys. Res.*, *88*, 10,359–10,370.

Savage, J., and J. Svarc (1997), Postseismic deformation associated with the 1992 M_w = 7.3 Landers earthquake, southern California, *J. Geophys. Res.*, *102*, 7565–7577.

Shelly, D. R., G. C. Beroza, S. Ide, and S. Nakamula (2006), Low-frequency earthquakes in Shikoku, Japan, and their relationship to episodic tremor and slip, *Nature*, *442*, 188–191.

Shelly, D. R., G. C. Beroza, and S. Ide (2007), Non-volcanic tremor and low-frequency earthquake swarms, *Nature*, *446*, 305–307.

Shibazaki, B., and T. Shimamoto (2007), Modelling of short-interval silent slip events in deeper subduction interfaces considering the frictional properties at the unstable-stable transition regime, *Geophys. J. Int.*, *171*, 191–205.

Shimizu, I. (1995), Kinetics of pressure solution creep in quartz: Theoretical considerations, *Tectonophysics*, *245*, 121–134.

Sibson, R. H. (1992), Fault-valve behavior and the hydrostatic lithostatic fluid pressure intereface, *Earth Sci. Rev.*, *32*, 141–144.

Sleep, N. (1995), Ductile creep, compaction, and rate and state dependent friction within major fault zones, *J. Geophys. Res.*, *100*, 13,065–13,080.

Sleep, N., and M. Blanpied (1992), Creep, compaction and the weak rheology of major faults, *Nature*, *359*, 687–692.

Szeliga, W., T. Melbourne, M. Miller, and V. Santillan (2004), Southern Cascadia episodic slow earthquakes, *Geophys. Res. Lett.*, *31*, L16602, doi:10.1029/2004GL020824.

Turcotte, D., and G. Schubert (2002), Rock rheology, in *Geodynamics*, 2nd ed., pp. 292–312. Cambridge Univ. Press, New York.

Yagi, Y., M. Kikuchi, and T. Nishimura (2003), Co-seismic slip, post-seismic slip, and largest aftershock associated with the 1994 Sanriku-harukaoki, Japan, earthquake, *Geophys. Res. Lett.*, *30*(22), 2177, doi:10.1029/2003GL018189.

J.-P. Ampuero, Seismological Laboratory, California Institute of Technology, 1200 East California Boulevard, Pasadena, CA 91125-2100, USA.

H. Perfettini, Institut de Recherche pour le Développement, Laboratoire des Mécanismes de Transfert en Géologie, 14 avenue Edouard Belin, F-31400 Toulouse, France. (hugo.perfettini@ird.fr)